

COLLABORATION-AWARE GRAPH CONVOLUTIONAL NETWORK FOR RECOMMENDER SYSTEMS

Yu Wang, Yuying Zhao, Yi Zhang, Tyler Derr

Department of Computer Science

Vanderbilt University

{yu.wang.1, yuying.zhao, yi.zhang, tyler.derr}@vanderbilt.edu

ABSTRACT

Graph Neural Networks (GNNs) have been successfully adopted in recommender systems by virtue of the message-passing that implicitly captures collaborative effect. Nevertheless, most of the existing message-passing mechanisms for recommendation are directly inherited from GNNs without scrutinizing whether the captured collaborative effect would benefit the prediction of user preferences. In this paper, we first analyze how message-passing captures the collaborative effect and propose a recommendation-oriented topological metric, Common Interacted Ratio (CIR), which measures the level of interaction between a specific neighbor of a node with the rest of its neighbors. After demonstrating the benefits of leveraging collaborations from neighbors with higher CIR, we propose a recommendation-tailored GNN, Collaboration-Aware Graph Convolutional Network (CAGCN), that goes beyond 1-Weisfeiler-Lehman(1-WL) test in distinguishing non-bipartite-subgraph-isomorphic graphs. Experiments on six benchmark datasets show that the best CAGCN variant outperforms the most representative GNN-based recommendation model, LightGCN, by nearly 10% in Recall@20 and also achieves around 80% speedup. Our code is available at <https://github.com/YuWVandy/CAGCN>

1 INTRODUCTION

Recommender systems aim to alleviate information overload by helping users discover items of interest (Covington et al., 2016; Ying et al., 2018) and have been widely deployed in real-world applications such as social media, advertising, and e-commerce. Given historical user-item interactions (e.g., click, purchase, review, and rate), the key of recommender systems is to leverage the collaborative effect (Ebesu et al., 2018; He et al., 2017; Wang et al., 2019) to predict how likely users will interact with items. A common paradigm for modeling collaborative effect is to first learn embeddings of users/items capable of recovering historical user-item interactions and then perform top-K recommendation based on the pairwise similarity between the learned user/item embeddings.

Since historical user-item interactions can be naturally represented as a bipartite graph with users/items being nodes and interactions being edges (Li & Chen, 2013; Wang et al., 2019; He et al., 2020) and given the unprecedented success of GNNs in learning node/graph representations (Kipf & Welling, 2017; Klicpera et al., 2019; Liu et al., 2020; Zhuang et al., 2022), recent research has started to leverage GNNs to learn user/item embeddings for the recommendation. Two pioneering works NGCF (Wang et al., 2019) and LightGCN (He et al., 2020) leverage graph convolutions to aggregate messages from local neighborhoods, which directly injects the collaborative signal into user/item embeddings. More recently, (Chen et al., 2021; Wu et al., 2021) explore the robustness and self-supervised learning of graph convolution for recommendation. However, the message-passing mechanisms in all previous recommendation models are directly inherited from GNNs without carefully justifying how collaborative signals are captured and whether the captured collaborative signals would benefit the prediction of user preference. Such ambiguous understanding on how the message-passing captures collaborative signals would pose the risk of learning uninformative or even harmful user/item representations when adopting GNNs in recommendation. For example, (Fan et al., 2021) shows that a large portion of user interactions cannot reflect their actual purchasing behaviors. In this case, blindly passing messages following existing styles of GNNs could capture harmful collab-

orative signals from these unreliable interactions, which corrupts user/item embeddings and hinders the performance of GNN-based models.

To avoid collecting noisy or even harmful collaborative signals in message-passing of traditional GNNs, existing work GTN (Fan et al., 2021) proposes to adaptively propagate user/item embeddings by adjusting the weight of edges based on items’ similarity to users’ main preferences (i.e., the trend). However, such similarity is still computed based on the learned embeddings that implicitly encode noisy collaborative signals from unreliable user-item interactions. Worse still, calculating edge weights based on user/item embeddings along the training on the fly is computationally prohibitive and hence prevents the model from being deployed in industrial-level recommendations. UltraGCN (Mao et al., 2021) approximates the message-passing by optimizing the link prediction loss through infinite-layer propagation, which squeezes noisy collaborative signals into embeddings through optimizing embeddings over unreliable interactions. SGCN (Chen et al., 2021) attaches the message-passing with a trainable stochastic binary mask to prune noisy edges. However, the jointly learning and the unbiased gradient estimator increases the computational load.

Despite the fundamental importance of capturing beneficial collaborative signals, the related studies are still in their infancy. To fill this crucial gap, we aim to demystify the collaborative effect captured by message-passing in GNNs and develop new insights towards customizing message-passing for recommendations. Furthermore, these insights motivate us to design a recommendation-tailored GNN, namely Collaboration-Aware Graph Convolutional Network(CAGCN), that selectively passes neighborhood information based on their Common Interacted Ratio (CIR) via the Collaboration-Aware Graph Convolution (CAGC). Our major contributions are listed as follows:

- **Novel Perspective on Collaborative Effect:** We demystify the collaborative effect by analyzing how message-passing helps users capture and leverage collaborative signals and when the captured collaborative signals are beneficial in computing users’ ranking over items.
- **Novel Recommendation-tailored Topological Metric:** We then propose a recommendation-tailored topological metric, Common Interacted Ratio (CIR), and demonstrate the capability of CIR to quantify the benefits of aggregating messages from neighborhoods.
- **Novel Graph Convolution beyond 1-WL for Recommendation:** We integrate CIR into message-passing and propose a novel Collaboration-Aware Graph Convolutional Network (CAGCN). Then we prove that it can go beyond 1-WL test in distinguishing non-bipartite-subgraph-isomorphic graphs, and show its superiority via experiments on real-world datasets including two newly collected datasets and provide an in-depth interpretation on its advantages.

We review related works in Section 2. In Section 3, we analyze the collaborative effect captured by message-passing and propose CIR to measure whether the captured collaborative effect would benefit the prediction of user preferences. Then, we introduce CAGCN in Section 4 and evaluate it in Section 5. Finally, we conclude and discuss future work in Section 6.

2 RELATED WORK

Collaborative Filtering & Recommendation. Collaborative filtering (CF) predicts users’ interest (filtering) by utilizing the preferences of other users with similar interests (collaborative) (Goldberg et al., 1992). Early CF methods used Matrix Factorization techniques (Rendle et al., 2009; Koren et al., 2009; Rendle et al., 2012; Tay et al., 2018) to capture CF effect via optimizing users/items’ embeddings over historical interactions. Stepping further, graph-based methods are proposed to either leverage topological constraints or message-passing to inject the CF effect into the user/item embeddings (He et al., 2020; Wang et al., 2019). ItemRank and BiRank (Gori et al., 2007; He et al., 2016) perform label propagation and compute users’ ranking based on structural proximity between the observed and the target items. To fix the issue of non-trainable user preference, HOP-Rec (Yang et al., 2018) combines the graph-based method, which better captures the collaboration, and the embedding-based method, which better optimizes the recommendation objective. Yet, interactions captured by random walks there do not fully explore the high-layer neighbors and multi-hop dependencies (Wang & Derr, 2021). By contrast, GNN-based methods are superior at encoding structural proximity (especially higher-order connection) in user/item embeddings (Wang et al., 2019; He et al., 2020). However, all existing GNN-based recommendation models directly borrow the graph convolution from node/graph classification without any recommendation-tailored

modification. Recent work (Chen et al., 2021; Fan et al., 2021) has already demonstrated that not all captured collaborations improve users’ ranking, which inspires us to design a new graph convolution that selectively passes messages based on the benefits of the provided collaborations.

Link Prediction. As a generalized version of recommendation, link prediction has become a central problem (Zhou, 2021) and finds applications in predicting drug interactions and recovering knowledge graphs (Rozemberczki et al., 2022; Nickel et al., 2015). Early studies adopt topological heuristics to score node pairs based on their connectivity (Leicht et al., 2006; Zhou et al., 2009; Newman, 2001). However, they made strong assumptions about the underline topological distribution and hence are not data-adaptive. To improve the hard-coded structural features introduced by heuristics, latent-based methods (Perozzi et al., 2014) are proposed to characterize underline topological patterns in node embeddings via implicitly injecting geometrical proximity by random walks (Grover & Leskovec, 2016) and explicitly regularizing over observed links (Perozzi et al., 2014). To fully leverage node features, GNN-based methods are proposed and achieve unprecedented success owing to the use of the neural network to extract task-related information and the message-passing to capture the topological pattern (Zhang & Chen, 2018; Pan et al., 2021; Zhao et al., 2022). Recently, efforts have been made towards developing expressive GNNs that can go beyond the 1-WL test (Zhao et al., 2021; Wijesinghe & Wang, 2021) and have already demonstrated their success in node/graph classification. Following this line, our goal is to develop a recommendation-tailored graph convolution with provably expressive power in predicting missing links between users and items.

3 ANALYSIS ON COLLABORATIVE EFFECT

Let $\mathcal{G} = (\mathcal{V}, \mathcal{E})$ be the user-item bipartite graph, where the node set $\mathcal{V} = \mathcal{U} \cup \mathcal{I}$ includes the user set \mathcal{U} and the item set \mathcal{I} . Following previous work (Wang et al., 2019; He et al., 2020; Mao et al., 2021), we only consider the implicit user-item interactions and denote them as edges \mathcal{E} where e_{pq} represents the edge between node p and q . The network topology is described by its adjacency matrix $\mathbf{A} \in \{0, 1\}^{|\mathcal{V}| \times |\mathcal{V}|}$, where $\mathbf{A}_{pq} = 1$ when $e_{pq} \in \mathcal{E}$, and $\mathbf{A}_{pq} = 0$ otherwise. Let \mathcal{N}_p^l denote the set of observed neighbors that are exactly l -hops away from p and $\mathcal{S}_p = (\mathcal{V}_{\mathcal{S}_p}, \mathcal{E}_{\mathcal{S}_p})$ be the neighborhood subgraph (Wijesinghe & Wang, 2021) induced in \mathcal{G} by $\tilde{\mathcal{N}}_p^1 = \mathcal{N}_p^1 \cup \{p\}$. We use \mathcal{P}_{pq}^l to denote the set of shortest paths of length l between node p and q and denote one of such paths as P_{pq}^l . Note that $\mathcal{P}_{pq}^l = \emptyset$ if it is impossible to have a path between p and q of length l , e.g., $\mathcal{P}_{11}^1 = \emptyset$ in an acyclic graph. Furthermore, we denote the initial embeddings of users/items as $\mathbf{E}^0 \in \mathbb{R}^{(n+m) \times d^0}$ where $\mathbf{e}_p^0 = \mathbf{E}_p^0$ is the node p ’s embedding and let d_p be the degree of node p .

Here we leverage LightGCN (He et al., 2020) as the canonical architecture to remove the nonlinear transformation and exclusively explore the collaborative effect captured by message-passing. Detailed model architecture and training of LightGCN are attached in Appendix A.1. As shown in Figure 1, LightGCN passes messages from user u /item i ’s neighbors within L -hops to u/i :

$$\mathbf{e}_u^{l+1} = d_u^{-0.5} \sum_{j \in \mathcal{N}_u^l} d_j^{-0.5} \mathbf{e}_j^l, \quad \mathbf{e}_i^{l+1} = d_i^{-0.5} \sum_{v \in \mathcal{N}_i^l} d_v^{-0.5} \mathbf{e}_v^l, \quad l \in \{0, 1, \dots, L\}. \quad (1)$$

Under this message-passing framework, we expect to answer the following two questions:

- Q_1 : How does message-passing capture the collaborative effect and leverage it in computing users’ ranking?
- Q_2 : When does the captured collaborative effect benefit to users’ ranking?

In the next section, We address Q_1 by theoretically deriving users’ ranking over items under the message-passing framework of LightGCN and address Q_2 by proposing the Common Interacted Ratio (CIR) to measure the benefits of leveraging collaborations from each neighbor in computing users’ ranking. The answers to the above two questions further motivate our design of Collaboration-Aware Graph Convolutional Network in Section 4.

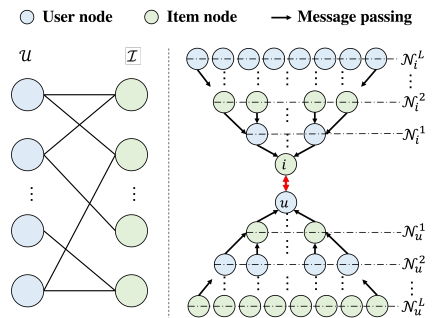


Figure 1: Computing user u ’s ranking over item i by leveraging all node information in u/i ’s computational graph.

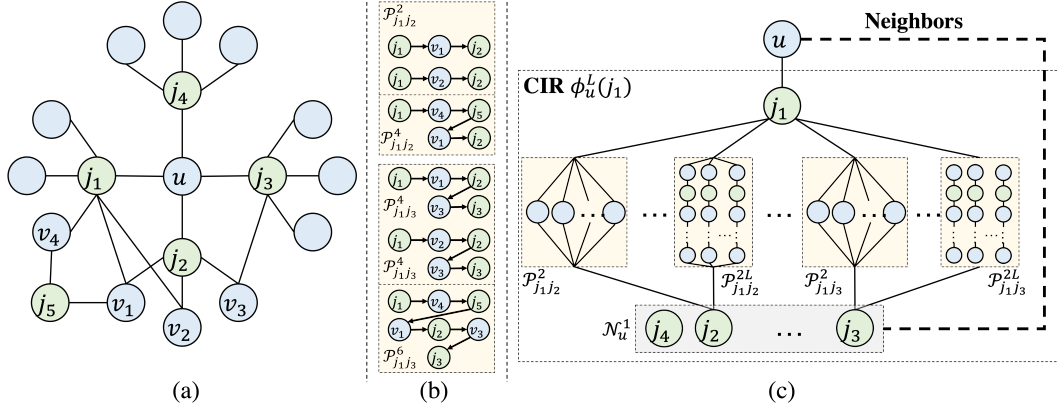


Figure 2: In (a)-(b), since j_1 has more interactions (paths) with (to) u 's neighborhood than j_4 , it is more representative of u 's purchasing behaviors rather than j_4 . In (c), we quantify the CIR between j_1 and u via the paths (and associated nodes) between j_1 and \mathcal{N}_u^1 .

3.1 HOW DOES MESSAGE-PASSING CAPTURE COLLABORATIVE EFFECT?

The collaborative effect occurs when the prediction of a user's preference relies on other users' preferences or items' properties (Ricci et al., 2011). Therefore, to answer \mathbf{Q}_1 , we need to seek whether we leverage other nodes' embeddings in computing a specific user's ranking over items. In the inference stage of LightGCN, we take the inner product between user u 's embedding and item i 's embedding after L -layers' message-passing to compute the ranking as¹:

$$y_{ui}^L = \left(\sum_{l_1=0}^L \sum_{j \in \mathcal{N}_u^{l_1}} \sum_{l_2=l_1}^L \beta_{l_2} \alpha_{ju}^{l_2} \mathbf{e}_j \right)^\top \left(\sum_{l_1=0}^L \sum_{v \in \mathcal{N}_i^{l_1}} \sum_{l_2=l_1}^L \beta_{l_2} \alpha_{vi}^{l_2} \mathbf{e}_v \right), \quad (2)$$

where $\alpha_{ju}^{l_2} = \sum_{P_{ju}^{l_2} \in \mathcal{P}_{ju}^{l_2}} \prod_{e_{pq} \in P_{ju}^{l_2}} d_p^{-0.5} d_q^{-0.5} (\alpha_{ju}^{l_2} = 0 \text{ if } \mathcal{P}_{ju}^{l_2} = \emptyset)$ denotes the total weight of all paths of length l_2 from j to u , $\mathcal{N}_u^0 = \{u\}$ and specifically, $\alpha_{uu}^0 = 1$. β_{l_2} is the weight measuring contributions of propagated embeddings at layer l_2 . Thus, based on Eq. (2), we present the answer to \mathbf{Q}_1 as \mathbf{A}_1 : L -layer LightGCN-based message-passing captures collaborations between pairs of nodes $\{(j, v) | j \in \bigcup_{l=0}^L \mathcal{N}_u^l, v \in \bigcup_{l=0}^L \mathcal{N}_i^l\}$, and the collaborative strength of each pair is determined by 1) $\mathbf{e}_j^\top \mathbf{e}_v^0$: embedding similarity between j and v , 2) $\{\alpha_{ju}^l\}_{l=0}^L (\{\alpha_{vi}^l\}_{l=0}^L)$: weight of all paths of length l to L from j to u (v to i), and 3) $\{\beta_l\}_{l=0}^L$: the weight of each layer.

3.2 WHEN ARE THE CAPTURED COLLABORATIVE EFFECT BENEFICIAL TO USERS' RANKING?

Even though users could leverage collaborations from other users/items as demonstrated above, we cannot guarantee all of these collaborations benefit the prediction of their preferences. For example, in Figure 2(a)-(b), u 's interacted item j_1 has more interactions (paths) to u 's neighborhoods than j_4 and hence is more representative of u 's purchasing behaviors (Fan et al., 2021; Chen et al., 2021). For each user u , we propose the **Common Interacted Ratio** to quantify the level of interaction between each of u 's specific neighboring item and u 's whole item neighborhood:

Definition 1. Common Interacted Ratio (CIR): For any item $j \in \mathcal{N}_u^1$ of user u , the CIR of j around u considering nodes up to $(L+1)$ -hops away from u , i.e., $\phi_u^L(j)$, is defined as the average interacted ratio of j with all neighboring items of u in \mathcal{N}_u^1 through paths of length $\leq 2L$:

$$\phi_u^L(j) = \frac{1}{|\mathcal{N}_u^1|} \sum_{i \in \mathcal{N}_u^1} \sum_{l=1}^L \beta^{2l} \sum_{P_{ji}^{2l} \in \mathcal{P}_{ji}^{2l}} \frac{1}{f(\{\mathcal{N}_k^1 | k \in P_{ji}^{2l}\})}, \forall j \in \mathcal{N}_u^1, \forall u \in \mathcal{U}, \quad (3)$$

where $\{\mathcal{N}_k^1 | k \in P_{ji}^{2l}\}$ represents the set of the 1-hop neighborhood of node k along the path P_{ji}^{2l} from node j to i of length $2l$. f is a normalization function to differentiate the importance of different paths in \mathcal{P}_{ji}^{2l} and its value depends on the neighborhood of each node along the path P_{ji}^{2l} . As shown

¹Detailed derivation is attached in Appendix A.3.1.

in Figure 2(c), $\phi_u^L(j_1)$ is decided by paths of length between 2 to $2L$. By configuring different L and f , $\sum_{P_{j_i}^{2l} \in \mathcal{P}_{j_i}^{2l}} \frac{1}{f(\{N_k^l | k \in P_{j_i}^{2l}\})}$ could express many existing graph similarity metrics (Leicht et al., 2006; Zhou et al., 2009; Newman, 2001; Salton, 1989; Liben-Nowell & Kleinberg, 2007) and we thoroughly discuss them in Appendix A.2. For simplicity, henceforth we denote $\phi_u^L(j)$ as $\phi_u(j)$.

We next empirically verify the importance of leveraging collaborations from neighbors with higher CIR by incrementally adding edges into an initially edge-less graph according to their CIR and visualizing the performance change. Specifically, we consider two settings, retraining and pretraining, which are visualized in Figure 3(a)-(b) and 3(c)-(d), respectively. Here we consider variants of CIR that we later define in Section 5.1 with further details in Appendix A.2.

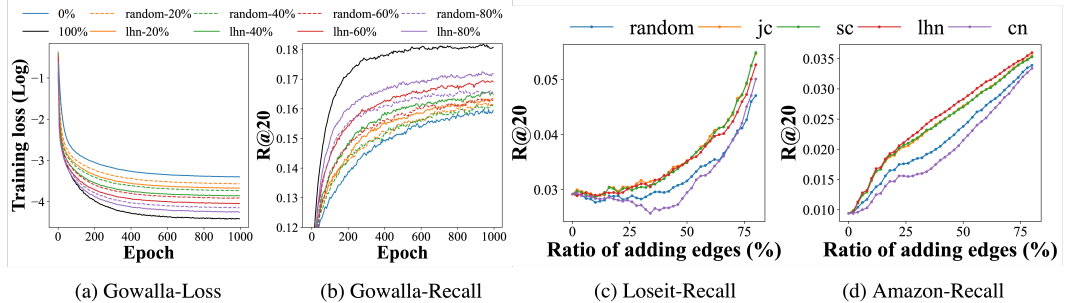


Figure 3: In (a)-(b), the training loss (the performance) is lower (higher) when adding edges according to CIRs than adding edges randomly under the same addition budget. In (c)-(d), the performance of adding edges according to CIRs increases faster than adding edges randomly after pre-training. We iteratively cycle over the nodes and for each of them, add its corresponding neighbor according to the corresponding CIR-variant until hitting the budget. More details are provided in Appendix A.7.1.

For the re-training setting, we first remove all observed edges in the training set to create the edge-less bipartite graph and then incrementally add edges according to their CIR and retrain user/item embeddings. In Figure 3(a)-(b), we evaluate the performance on the newly constructed bipartite graph under different edge budgets. Clearly, the training loss/performance becomes lower/higher when adding more edges because message-passing captures more collaborative effects. Furthermore, since edges with higher CIR connect neighbors with more connections to the whole neighborhood, optimizing embeddings of nodes incident to these edges pull the whole neighborhood closer and hence leads to the lower training loss over neighborhoods’ connections, which causes the overall lower training loss in Figure 3(a). In Figure 3(b), we observe that under the same adding budget, adding according to CIRs achieves higher performance than adding randomly. It is because neighbors with higher interactions with the whole neighborhood are more likely to have higher interactions with neighbors to be predicted (We empirically verify this in Appendix A.4.). Then for each user, maximizing its embedding similarity to its training neighbors with higher CIR will indirectly improve its similarity to its to-be-predicted neighbors, which leads to lower population risk and higher generalization/performance.

For the pre-training setting, we first pre-train user/item embeddings on the original entire bipartite graph and then propagate the pre-trained embeddings on the newly constructed bipartite graph under different edge budgets. This setting is more realistic since in the real digital world, with the exponential interactions continually coming in (Wang et al., 2020) while the space used for storage is limited, we are forced to keep only partial interactions and the pre-trained user/item embeddings. Figure 3(c)-(d) demonstrates that under the same adding budget, keeping edges according to CIR leads to higher performance than keeping randomly, which further verifies the effectiveness of CIR in quantifying the edge importance. An interesting observation is that adding more edges cannot always bring performance gain as shown in Figure 3(d) when the ratio of added edges is between 0%-20%. We hypothesize that due to the low density of the Loseit dataset, only when users receive messages from neighbors beyond a certain level can we guarantee the learned user representation is meaningful. Different variants of CIR lead to different increasing speeds of the performance. For example, sc is faster on Loseit in Figure 3(c) while lhn is faster on Amazon in Figure 3(d). In addition, the faster improvement by keeping edges according to CIR also indicates its potential in devising a better strategy of pruning edges in the setting of continual learning (Wang et al., 2022).

From the above analysis, we summarize the answer A_2 to Q_2 as: *Leveraging collaborations from u ’s neighboring node j with higher CIR $\phi_u(j)$ would cause more benefits to u ’s ranking.*

4 COLLABORATION-AWARE GRAPH CONVOLUTIONAL NETWORKS

The former section demonstrates that passing messages according to neighbors’ CIR is crucial in improving users’ ranking. This motivates us to propose a new graph convolution operation, Collaboration-Aware Graph Convolution (CAGC), which passes node messages based on the benefits of their provided collaborations. Furthermore, we wrap the proposed CAGC within LightGCN and develop the Collaboration-Aware Graph Convolutional Network (CAGCN).

4.1 COLLABORATION-AWARE GRAPH CONVOLUTION

The core idea of CAGC is to strengthen/weaken the messages passed from neighbors with higher/lower CIR to center nodes. To achieve this, we compute the edge weight as:

$$\Phi_{ij} = \begin{cases} \phi_i(j), & \text{if } \mathbf{A}_{ij} > 0 \\ 0, & \text{if } \mathbf{A}_{ij} = 0 \end{cases}, \forall i, j \in \mathcal{V} \quad (4)$$

where $\phi_i(j)$ is the CIR of neighboring node j centering around i . Note that unlike the symmetric graph convolution $\mathbf{D}^{-0.5}\mathbf{A}\mathbf{D}^{-0.5}$ used in LightGCN, here Φ is unsymmetric. This is rather interpretable: the interacting level of node j with i ’s neighborhood is likely to be different from the interacting level of node i with j ’s neighborhood. We further normalize Φ and combine it with the LightGCN convolution:

$$\mathbf{e}_i^{l+1} = \sum_{j \in \mathcal{N}_i^1} g(\gamma_i \frac{\Phi_{ij}}{\sum_{k \in \mathcal{N}_i^1} \Phi_{ik}}, d_i^{-0.5} d_j^{-0.5}) \mathbf{e}_j^l, \forall i \in \mathcal{V} \quad (5)$$

where γ_i is a coefficient that varies the total amount of message flowing to each node i and controls the embedding magnitude of that node (Park et al., 2020). g is a function combining the edge weights computed based on CIR and LightGCN. We could either learn g by parametrization (e.g., concatenating these two types of propagated embeddings and applying MLP) or set g based on prior knowledge (e.g., weighted sum of these two propagated embeddings). Next, we prove that for a certain choice of g and γ_i , CAGCN can go beyond 1-WL test in distinguishing non-bipartite-subgraph-isomorphic graphs. First, we prove the equivalence between the subtree-isomorphism and the subgraph-isomorphism in bipartite graphs:

Theorem 1. *In bipartite graphs, two subgraphs that are subtree-isomorphic if and only if they are subgraph-isomorphic.*

The definition of subtree-isomorphism/subgraph-isomorphism and the proof of Theorem 1 are included in Appendix A.3.2. Since 1-WL test can distinguish subtree-isomorphic graphs (Wijesinghe & Wang, 2021), the equivalence between these two isomorphisms indicates that in bipartite graphs, both of the subtree-isomorphic graphs and subgraph-isomorphic graphs can be distinguished by 1-WL test. Therefore, to go beyond 1-WL in bipartite graphs, we propose a novel bipartite-subgraph-isomorphism in Definition 2, which is even harder to be distinguished than the subgraph-isomorphism by 1-WL test.

Definition 2. Bipartite-subgraph-isomorphism: \mathcal{S}_u and \mathcal{S}_i are bipartite-subgraph-isomorphic, denoted as $\mathcal{S}_u \cong_{bi\text{-subgraph}} \mathcal{S}_i$, if there exists a bijective mapping $h : \tilde{\mathcal{N}}_u^1 \cup \mathcal{N}_u^2 \rightarrow \tilde{\mathcal{N}}_i^1 \cup \mathcal{N}_i^2$ such that $h(u) = i$ and $\forall v, v' \in \tilde{\mathcal{N}}_u^1 \cup \mathcal{N}_u^2, e_{vv'} \in \mathcal{E} \iff e_{h(v)h(v')} \in \mathcal{E}$ and $\mathbf{e}_v^l = \mathbf{e}_{h(v)}^l, \mathbf{e}_{v'}^l = \mathbf{e}_{h(v')}^l$.

Theorem 2. *Let M be a GNN with sufficient number of CAGC-based convolution layers defined by Eq. (5). If g is MLP, then M is strictly more expressive than 1-WL in distinguishing subtree-isomorphic yet non-bipartite-subgraph-isomorphic graphs.*

The detailed proof of Theorem 2 is attached in Appendix A.3.2. It indicates that GNNs whose aggregation scheme is CAGC can distinguish non-bipartite-subgraph-isomorphic graphs that are indistinguishable by 1-WL.

4.2 MODEL ARCHITECTURE AND COMPLEXITY ANALYSIS

We expect the designed model to be light and trained easily. Figure 8 compares the architecture of CAGCN and LightGCN. Except for the message-passing, all other components of CAGCN including the average pooling and the model training are exactly the same as LightGCN, which are detaily

covered in Appendix A.1. Our model shares the same time/space complexity with LightGCN in all components except the extra computation of Φ , the time of computing which during preprocessing stage is minor compared with the whole training process. Detailed complexity comparison of our CAGC and all baselines is included in Appendix A.5.

5 EXPERIMENTS

In this section, we conduct experiments to evaluate the effectiveness of our proposed CAGCN.

5.1 EXPERIMENTAL SETTINGS

Datasets. We validate the proposed CAGC and CAGCN on four widely used benchmark datasets in recommender systems, including Gowalla, Yelp, Amazon, and MI-1M (He et al., 2020; Wang et al., 2019). Moreover, we collect two extra datasets, Loseit and News to further demonstrate the superiority of our proposed model in even broader domains of user-item interactions. Statistics of these datasets are thoroughly described in Appendix A.6.1.

Baseline methods. We compare our proposed CAGCN with the following baselines: MF, NGCF, LightGCN, UltraGCN, GTN (Rendle et al., 2012; Wang et al., 2019; He et al., 2020; Mao et al., 2021; Fan et al., 2021). Details of the above baselines are clarified in Appendix A.6.2. Note that the purpose here is to evaluate how effective our aggregation scheme can learn embeddings for the recommendation, we only compare the proposed CAGCN with the baselines that focus on the operation of graph convolution (besides the classic MF) including the state-of-the-art GNN-based recommendation models (i.e., UltraGCN and GTN).

CAGCN-variants. For CAGCN, we set $\gamma_i = \sum_{r \in \mathcal{N}_i^+} d_i^{-0.5} d_r^{-0.5}$ to ensure that the total edge weights for messages received by each node are the same as LightGCN. For CAGCN*, we set $\gamma_i = \gamma$ as a constant controlling the trade-off between contributions from message-passing by LightGCN and by CAGC. We term the model variant as CAGCN(*)-jc if we use Jaccard Similarity (JC) (Liben-Nowell & Kleinberg, 2007) to compute Φ . The same rule applies to other topological metrics listed in Appendix A.2. Equations about CAGCN and CAGCN* are provided in Appendix A.6.3.

Experimental setup. Recall@20 (R@20) and Normalized Discounted Cumulative Gain (N@20) (Wang et al., 2019) are adopted to evaluate all models. We report the average of R@20 and N@20 over all users in the test set. In the inference phase, we treat items that the user has never interacted with in the training set as candidate items. Further details are provided in Appendix A.6.4.

5.2 PERFORMANCE COMPARISON

We first compare our proposed CAGCN-variants with LightGCN. In Table 1, CAGCN-jc/sc/lhn achieves higher performance than LightGCN because we aggregate more information from nodes with higher CIR(jc, sc, lhn) that bring more beneficial collaborations as justified in Section 3.2. CAGCN-cn generally performs worse than LightGCN because nodes having more common neighbors with other nodes tend to have high degrees and blindly aggregating information more from these nodes would cause false-positive link prediction. Since different datasets exhibit different patterns of 2nd-order connectivity, there is no fixed topological metric that performs the best among all datasets. For example, CAGCN-jc performs better than CAGCN-sc on Yelp and News, while worse on Gowalla, MI-1M.

Then, we compare CAGCN*-variants with other competing baselines. We omit CAGCN*-cn here due to the worse performance of CAGCN-cn than LightGCN. We can see that CAGCN*-jc/sc almost consistently achieves higher performance than other baselines except for UltraGCN on Amazon. This is because UltraGCN allows multiple negative samples for each positive interaction, e.g., 500 negative samples here on Amazon², which lowers the efficiency as we need to spend more time preparing a large number of negative samples per epoch. Among the baselines, UltraGCN exhibits the strongest performance because it approximates the infinite layers of message passing and constructs the user-user graphs to capture 2nd-order connectivity. LightGCN and NGCF perform better than MF since they inject the collaborative effect directly through message-passing.

²UltraGCN uses 1500/800/500/200 negative samples for Gowalla/Yelp2018/Amazon/MI-1M datasets.

Table 1: Performance comparison of CAGCN(*) with baselines. The best and runner-up results are colored in red and blue. The comparison with GTN is in Table 2 to align with GTN’s own setting.

Model	Metric	MF	NGCF	LightGCN	UltraGCN	CAGCN				CAGCN*		
						-jc	-sc	-cn	-lhn	-jc	-sc	-lhn
Gowalla	R@20	0.1554	0.1563	0.1817	0.1867	0.1825	0.1826	0.1632	0.1821	0.1878	0.1878	0.1857
	N@20	0.1301	0.1300	0.1570	0.1580	0.1575	0.1577	0.1381	0.1577	0.1591	0.1588	0.1563
Yelp2018	R@20	0.0539	0.0596	0.0659	0.0675	0.0674	0.0671	0.0661	0.0661	0.0708	0.0711	0.0676
	N@20	0.0460	0.0489	0.0554	0.0553	0.0564	0.0560	0.0546	0.0555	0.0586	0.0590	0.0554
Amazon	R@20	0.0337	0.0336	0.0420	0.0682	0.0435	0.0435	0.0403	0.0422	0.0510	0.0506	0.0457
	N@20	0.0265	0.0262	0.0331	0.0553	0.0343	0.0342	0.0321	0.0333	0.0403	0.0400	0.0361
MI-1M	R@20	0.2604	0.2619	0.2752	0.2783	0.2780	0.2786	0.2730	0.2760	0.2822	0.2827	0.2799
	N@20	0.2697	0.2729	0.2820	0.2638	0.2871	0.2881	0.2818	0.2871	0.2775	0.2776	0.2745
Loseit	R@20	0.0539	0.0574	0.0588	0.0621	0.0622	0.0625	0.0502	0.0592	0.0654	0.0658	0.0658
	N@20	0.0420	0.0442	0.0465	0.0446	0.0474	0.0470	0.0379	0.0461	0.0486	0.0484	0.0489
News	R@20	0.1942	0.1994	0.2035	0.2034	0.2135	0.2132	0.1726	0.2084	0.2182	0.2172	0.2053
	N@20	0.1235	0.1291	0.1311	0.1301	0.1385	0.1384	0.1064	0.1327	0.1405	0.1414	0.1311
Avg. Rank	R@20	9.83	9.17	7.33	4.17	4.67	4.33	8.83	6.17	1.67	1.50	3.33
	N@20	9.50	9.17	5.83	6.00	3.67	4.00	8.33	5.00	2.50	2.50	5.17

To align the setting with GTN, we increase the embedding size d^0 to 256 following (Fan et al., 2021)³ and observe the consistent superiority of our model over GTN in Table 2. This is because in GTN (Fan et al., 2021), the edge weights for message-passing are still computed based on node embeddings that implicitly encode noisy collaborative signals from unreliable interactions. Conversely, our CAGCN* directly alleviates the propagation on unreliable interactions based on its CIR value, which removes noisy interactions from the source.

Table 2: Performance comparison.

Model	Metric	GTN	CAGCN*		
			-jc	-sc	-lhn
Gowalla	R@20	0.1870	0.1901	0.1899	0.1885
	N@20	0.1588	0.1604	0.1603	0.1576
Yelp2018	R@20	0.0679	0.0731	0.0729	0.0689
	N@20	0.0554	0.0605	0.0601	0.0565
Amazon	R@20	0.0450	0.0573	0.0575	0.0520
	N@20	0.0346	0.0456	0.0458	0.0409

Table 3: Efficiency comparison.

Model	Stage	Gowalla	Yelp	Amazon	MI-1M	Loseit	News
LightGCN	Training	16432.0	28788.0	81976.5	18872.3	39031.0	13860.8
	Preprocess	167.4	281.6	1035.8	33.8	31.4	169.0
CAGCN*	Training	2963.2	1904.4	1983.9	11304.7	10417.7	1088.4
	Total	3130.6	2186.0	3019.7	11338.5	10449.1	1157.4
Improve	Training	82.0%	93.4%	97.6%	40.1%	73.3%	92.1%
	Total	80.9%	92.4%	96.3%	39.9%	73.2%	91.6%

5.3 EFFICIENCY COMPARISON

Here we compare the efficiency of the proposed CAGCN(*) with other baselines. To guarantee a fair comparison, we use a uniform code framework implemented ourselves for all models and run them on the same machine with Ubuntu 20.04 system, AMD Ryzen 9 5900 12-Core Processor (3.0 GHz), 128 GB RAM and GPU NVIDIA GeForce RTX 3090. We report the R@20 on Yelp and N@20 on Loseit of the best CAGCN(*) variant based on Table 1. We track the performance and the training time per 5 epochs. Complete results are included in Appendix A.7.3. In Figure 4(a)-(b), CAGCN achieves higher performance than LightGCN in less time. We hypothesize that for each user, its neighbors with higher interactions with its whole neighborhood would also have higher interactions with its interacted but unobserved neighbors. Then as CAGC aggregate more information from these neighbors, it indirectly enables the user to aggregate more information from its to-be-predicted neighbors as justified in Appendix A.4. Moreover, CAGCN* achieves even higher performance with even less time since we combine two views of propagation together. In addition, We report the first time that our best CAGCN* variant and GTN achieves the best performance of LightGCN on each dataset in Table 3. We also report the time for pre-calculating the CIR matrix Φ . We could see CAGCN* spends significantly less time to achieve the same best performance as LightGCN, which highlights the broad prospects to deploy CAGCN* in real-world recommendations.

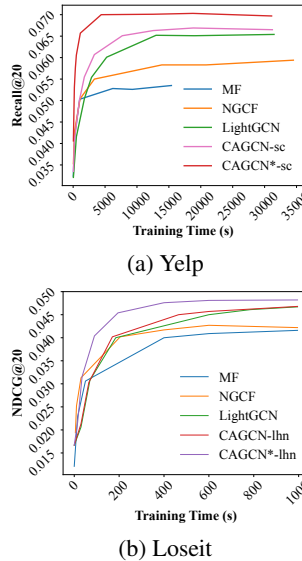


Figure 4: Training time (s) of different models.

³As the user/item embedding is a significant hyperparameter, it is crucial to ensure the same embedding size when comparing models; thus, we separately compare against GTN using their larger embedding size.

5.4 FURTHER PROBE

Performance grouped by node degrees. Here we group nodes by degree and visualize the average performance of each group. Comparing non-graph-based models (e.g., MF), graph-based models (e.g., LightGCN, CAGCN(*)) achieve higher performance for lower degree nodes [0, 300) while lower performance for higher degree nodes [300, Inf). Since node degree follows the power-law distribution (Stephen & Toubia, 2009), the average performance of graph-based models is still higher than MF. On one hand, graph-based models leverage neighborhood to augment the weak supervision for low-degree nodes. On the other hand, they introduce noisy interactions for higher-degree nodes. In addition, the opposite performance trends between NDCG and Recall indicate that different evaluation metrics have different sensitivity to node degrees.

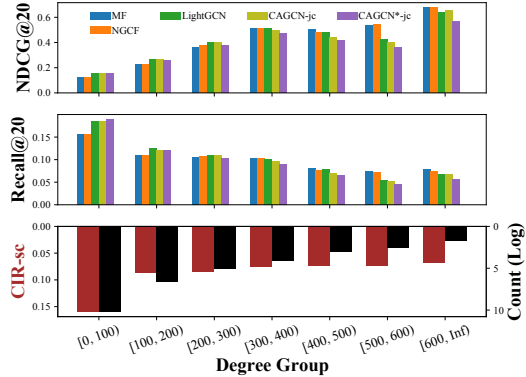


Figure 5: The performance of each model w.r.t. node degree on Gowalla. We observe a similar trend on Yelp in Appendix A.7.4.

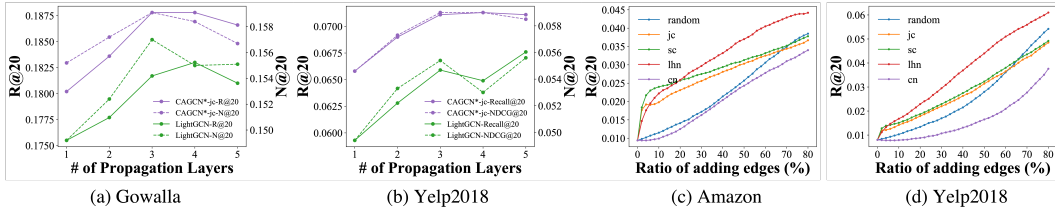


Figure 6: In (a)-(b), we increase the propagation layers from 1 to 5 and evaluate the performance on Gowalla and Yelp2018. Clearly, the performance first increases since we capture high-layer neighborhood information and then decreases due to over-smoothing. In (c)-(d), we add the global top edges according to their CIR to the bipartite graph and evaluate the performance. More details are provided in Appendix A.7.2.

Impacts of changing propagation layers. Figure 6(a)-(b) visualize the performance of CAGCN* and LightGCN when we increase the propagation layer from 1 to 5. Clearly, the performance first increases as the layer increases from 1 to 3 due to the incorporation of high-layer neighborhood information and then decreases due to over-smoothing. More importantly, our CAGCN* is always better than LightGCN at all propagation layers.

Adding edges globally according to CIR. Figure 6(c)-(d) visualizes the performance change when we add edges randomly and according to CIR. We select the global top edges (rather than for each center node) according to their CIR and then evaluate the LightGCN with the pre-trained user-item embeddings. In the first stage, we observe a similar trend that adding edges according to JC, SC, and LHN lead to faster performance gain. However, since we don't cycle over each node as we do in Appendix A.7.1, we would keep adding so many edges with larger CIR to the same node, which may not maximize our performance benefit when the metric is calculated by averaging over all nodes.

6 CONCLUSION

In this paper, we find that message-passing captures the collaborative effect by passing neighboring embeddings and the strength depends on the embedding similarity and the weight of paths. Then, we further propose the Common Interacted Ratio (CIR) and empirically verify that leveraging collaborations from neighbors with higher CIR contributes more to users' ranking. Based on CIR, we propose Collaboration-aware Graph Convolution (CAGC) to selectively pass messages from neighbors and prove its superiority over 1-WL in distinguishing non-bipartite-subgraph-isomorphic graphs. Experimental results demonstrate the advantages of the proposed CAGC and specifically, CAGCN* outperforms LightGCN He et al. (2020), by 9% in Recall@20 with more than 79% speedup.

REFERENCES

- Huiyuan Chen, Lan Wang, Yusan Lin, Chin-Chia Michael Yeh, Fei Wang, and Hao Yang. Structured graph convolutional networks with stochastic masks for recommender systems. In *Proceedings of the 44th International ACM SIGIR Conference on Research and Development in Information Retrieval*, pp. 614–623, 2021.
- Huiyuan Chen, Chin-Chia Michael Yeh, Fei Wang, and Hao Yang. Graph neural transport networks with non-local attentions for recommender systems. In *Proceedings of the ACM Web Conference 2022*, pp. 1955–1964, 2022a.
- Huiyuan Chen, Kaixiong Zhou, Kwei-Herng Lai, Xia Hu, Fei Wang, and Hao Yang. Adversarial graph perturbations for recommendations at scale. 2022b.
- Paul Covington, Jay Adams, and Emre Sargin. Deep neural networks for youtube recommendations. In *Proceedings of the 10th ACM conference on recommender systems*, pp. 191–198, 2016.
- Travis Ebesu, Bin Shen, and Yi Fang. Collaborative memory network for recommendation systems. In *The 41st international ACM SIGIR conference on research & development in information retrieval*, pp. 515–524, 2018.
- Wenqi Fan, Xiaorui Liu, Wei Jin, Xiangyu Zhao, Jiliang Tang, and Qing Li. Graph trend networks for recommendations. *arXiv preprint arXiv:2108.05552*, 2021.
- Hao-Ming Fu, Patrick Poirson, Kwot Sin Lee, and Chen Wang. Revisiting neighborhood-based link prediction for collaborative filtering. *arXiv preprint arXiv:2203.15789*, 2022.
- David Goldberg, David Nichols, Brian M Oki, and Douglas Terry. Using collaborative filtering to weave an information tapestry. *Communications of the ACM*, 35(12):61–70, 1992.
- Marco Gori, Augusto Pucci, V Roma, and I Siena. Itemrank: A random-walk based scoring algorithm for recommender engines. In *IJCAI*, volume 7, pp. 2766–2771, 2007.
- Aditya Grover and Jure Leskovec. node2vec: Scalable feature learning for networks. In *Proceedings of the 22nd ACM SIGKDD international conference on Knowledge discovery and data mining*, pp. 855–864, 2016.
- Ruining He and Julian McAuley. Vbpr: visual bayesian personalized ranking from implicit feedback. In *Proceedings of the AAAI Conference on Artificial Intelligence*, volume 30, 2016.
- Xiangnan He, Ming Gao, Min-Yen Kan, and Dingxian Wang. Birank: Towards ranking on bipartite graphs. *IEEE Transactions on Knowledge and Data Engineering*, 29(1):57–71, 2016.
- Xiangnan He, Lizi Liao, Hanwang Zhang, Liqiang Nie, Xia Hu, and Tat-Seng Chua. Neural collaborative filtering. In *Proceedings of the 26th international conference on world wide web*, pp. 173–182, 2017.
- Xiangnan He, Kuan Deng, Xiang Wang, Yan Li, Yongdong Zhang, and Meng Wang. Lightgcn: Simplifying and powering graph convolution network for recommendation. In *Proceedings of the 43rd International ACM SIGIR conference on research and development in Information Retrieval*, pp. 639–648, 2020.
- Thomas N. Kipf and Max Welling. Semi-supervised classification with graph convolutional networks. In *ICLR*, 2017.
- Johannes Klicpera, Aleksandar Bojchevski, and Stephan Günnemann. Predict then propagate: Graph neural networks meet personalized pagerank. In *7th International Conference on Learning Representations, ICLR*, 2019.
- Yehuda Koren, Robert Bell, and Chris Volinsky. Matrix factorization techniques for recommender systems. *Computer*, 42(8):30–37, 2009.
- Elizabeth A Leicht, Petter Holme, and Mark EJ Newman. Vertex similarity in networks. *Physical Review E*, 73(2):026120, 2006.

- Xin Li and Hsinchun Chen. Recommendation as link prediction in bipartite graphs: A graph kernel-based machine learning approach. *Decision Support Systems*, 54(2):880–890, 2013.
- David Liben-Nowell and Jon Kleinberg. The link-prediction problem for social networks. *Journal of the American society for information science and technology*, 58(7):1019–1031, 2007.
- Meng Liu, Hongyang Gao, and Shuiwang Ji. Towards deeper graph neural networks. In *Proceedings of the 26th ACM SIGKDD international conference on knowledge discovery & data mining*, pp. 338–348, 2020.
- Kelong Mao, Jieming Zhu, Xi Xiao, Biao Lu, Zhaowei Wang, and Xiuqiang He. Ultragen: Ultra simplification of graph convolutional networks for recommendation. In *Proceedings of the 30th ACM International Conference on Information & Knowledge Management*, pp. 1253–1262, 2021.
- Mark EJ Newman. Clustering and preferential attachment in growing networks. *Physical review E*, 64(2):025102, 2001.
- Maximilian Nickel, Kevin Murphy, Volker Tresp, and Evgeniy Gabrilovich. A review of relational machine learning for knowledge graphs. *Proceedings of the IEEE*, 104(1):11–33, 2015.
- Liming Pan, Cheng Shi, and Ivan Dokmanić. Neural link prediction with walk pooling. *arXiv preprint arXiv:2110.04375*, 2021.
- Dongmin Park, Hwanjun Song, Minseok Kim, and Jae-Gil Lee. Trap: Two-level regularized autoencoder-based embedding for power-law distributed data. In *Proceedings of The Web Conference 2020*, pp. 1615–1624, 2020.
- Bryan Perozzi, Rami Al-Rfou, and Steven Skiena. Deepwalk: Online learning of social representations. In *Proceedings of the 20th ACM SIGKDD international conference on Knowledge discovery and data mining*, pp. 701–710, 2014.
- Steffen Rendle, Christoph Freudenthaler, Zeno Gantner, and Lars Schmidt-Thieme. Bpr: Bayesian personalized ranking from implicit feedback. In *Proceedings of the Twenty-Fifth Conference on Uncertainty in Artificial Intelligence*, pp. 452–461, 2009.
- Steffen Rendle, Christoph Freudenthaler, Zeno Gantner, and Lars Schmidt-Thieme. Bpr: Bayesian personalized ranking from implicit feedback. *arXiv preprint arXiv:1205.2618*, 2012.
- Francesco Ricci, Lior Rokach, and Bracha Shapira. Introduction to recommender systems handbook. In *Recommender systems handbook*. Springer, 2011.
- Benedek Rozemberczki, Charles Tapley Hoyt, Anna Gogleva, Piotr Grabowski, Klas Karis, Andrej Lamov, Andriy Nikolov, Sebastian Nilsson, Michael Ughetto, Yu Wang, et al. Chemicalx: A deep learning library for drug pair scoring. *arXiv preprint arXiv:2202.05240*, 2022.
- Gerard Salton. Automatic text processing: The transformation, analysis, and retrieval of. *Reading: Addison-Wesley*, 169, 1989.
- Andrew T Stephen and Olivier Toubia. Explaining the power-law degree distribution in a social commerce network. *Social Networks*, 31(4):262–270, 2009.
- Yi Tay, Luu Anh Tuan, and Siu Cheung Hui. Latent relational metric learning via memory-based attention for collaborative ranking. In *WWW*, pp. 729–739, 2018.
- Chen Wang, Yuheng Qiu, Dasong Gao, and Sebastian Scherer. Lifelong graph learning. In *Proceedings of the IEEE/CVF Conference on Computer Vision and Pattern Recognition*, pp. 13719–13728, 2022.
- Junshan Wang, Guojie Song, Yi Wu, and Liang Wang. Streaming graph neural networks via continual learning. In *Proceedings of the 29th ACM International Conference on Information & Knowledge Management*, pp. 1515–1524, 2020.
- Xiang Wang, Xiangnan He, Meng Wang, Fuli Feng, and Tat-Seng Chua. Neural graph collaborative filtering. In *Proceedings of the 42nd international ACM SIGIR conference on Research and development in Information Retrieval*, pp. 165–174, 2019.

- Yu Wang and Tyler Derr. Tree decomposed graph neural network. In *Proceedings of the 30th ACM International Conference on Information & Knowledge Management*, pp. 2040–2049, 2021.
- William Webber, Alistair Moffat, and Justin Zobel. A similarity measure for indefinite rankings. *ACM Transactions on Information Systems (TOIS)*, 28(4):1–38, 2010.
- Asiri Wijesinghe and Qing Wang. A new perspective on” how graph neural networks go beyond weisfeiler-lehman?”. In *ICLR*, 2021.
- Jiancan Wu, Xiang Wang, Fuli Feng, Xiangnan He, Liang Chen, Jianxun Lian, and Xing Xie. Self-supervised graph learning for recommendation. In *Proceedings of the 44th International ACM SIGIR Conference on Research and Development in Information Retrieval*, pp. 726–735, 2021.
- Keyulu Xu, Weihua Hu, Jure Leskovec, and Stefanie Jegelka. How powerful are graph neural networks? *arXiv preprint arXiv:1810.00826*, 2018.
- Jheng-Hong Yang, Chih-Ming Chen, Chuan-Ju Wang, and Ming-Feng Tsai. Hop-rec: high-order proximity for implicit recommendation. In *Proceedings of the 12th ACM Conference on Recommender Systems*, pp. 140–144, 2018.
- Rex Ying, Ruining He, Kaifeng Chen, Pong Eksombatchai, William L Hamilton, and Jure Leskovec. Graph convolutional neural networks for web-scale recommender systems. In *Proceedings of the 24th ACM SIGKDD*, pp. 974–983, 2018.
- Muhan Zhang and Yixin Chen. Link prediction based on graph neural networks. *Advances in neural information processing systems*, 31, 2018.
- Lingxiao Zhao, Wei Jin, Leman Akoglu, and Neil Shah. From stars to subgraphs: Uplifting any gnn with local structure awareness. In *International Conference on Learning Representations*, 2021.
- Tong Zhao, Gang Liu, Daheng Wang, Wenhao Yu, and Meng Jiang. Learning from counterfactual links for link prediction. In *International Conference on Machine Learning*, pp. 26911–26926. PMLR, 2022.
- Tao Zhou. Progresses and challenges in link prediction. *Iscience*, 24(11):103217, 2021.
- Tao Zhou, Linyuan Lü, and Yi-Cheng Zhang. Predicting missing links via local information. *The European Physical Journal B*, 71(4):623–630, 2009.
- Zixu Zhuang, Sheng Wang, Liping Si, Kai Xuan, Zhong Xue, Dinggang Shen, Lichi Zhang, Weiwu Yao, and Qian Wang. Local graph fusion of multi-view mr images for knee osteoarthritis diagnosis. In *International Conference on Medical Image Computing and Computer-Assisted Intervention*, pp. 554–563. Springer, 2022.

A APPENDIX

A.1 MODEL ARCHITECTURE AND TRAINING OF LIGHTGCN

As stated in Section 3, we leverage LightGCN to solely study the effect of message-passing in capturing collaborative effect since it does not include any nonlinear transformation. Here we introduce the framework of LightGCN. Given the initial user and item embeddings $\mathbf{E}^0 \in \mathbb{R}^{(n+m) \times d^0}$, LightGCN performs L layers’ message-passing as:

$$\mathbf{E}^l = \tilde{\mathbf{A}}^l \mathbf{E}^0, \quad \forall l \in \{1, 2, \dots, L\}, \quad (6)$$

where $\tilde{\mathbf{A}} = \mathbf{D}^{-0.5} \mathbf{A} \mathbf{D}^{-0.5}$ and \mathbf{D} is the degree matrix of \mathbf{A} . Then all L layers propagated embeddings are aggregated together by mean-pooling:

$$\mathbf{E}^L = \frac{1}{(L+1)} \sum_{l=0}^L \mathbf{E}^l. \quad (7)$$

In the training stage, for each observed user-item interaction (u, i) , LightGCN randomly samples a negative item i^- that u has never interacted with before, and forms the triple (u, i, i^-) , which collectively forms the set of observed training triples \mathcal{O} . After that, the ranking scores of the user over these two items are computed as $y_{ui} = \mathbf{e}_u^\top \mathbf{e}_i$ and $y_{ui^-} = \mathbf{e}_u^\top \mathbf{e}_{i^-}$, which are finally used in optimizing the pairwise Bayesian Personalized Ranking (BPR) loss (Rendle et al., 2012):

$$\mathcal{L}_{\text{BPR}} = \sum_{(u, i, i^-) \in \mathcal{O}} -\ln \sigma(y_{ui} - y_{ui^-}), \quad (8)$$

where $\sigma(\cdot)$ is the Sigmoid function, and here we omit the L_2 regularization term since it is mainly for alleviating overfitting and has no influence on the collaborative effect captured by message passing.

A.2 GRAPH TOPOLOGICAL METRICS FOR CIR

Here we demonstrate that by configuring different f and L , $\phi_u^L(j)$ can express many existing graph similarity metrics.

$$\phi_u^L(j) = \frac{1}{|\mathcal{N}_u^1|} \sum_{i \in \mathcal{N}_u^1} \sum_{l=1}^L \beta^l \sum_{P_{ji}^{2l} \in \mathcal{P}_{ji}^{2l}} \frac{1}{f(\{\mathcal{N}_k^1 | k \in P_{ji}^{2l}\})}, \forall j \in \mathcal{N}_u^1, \forall u \in \mathcal{U}, \quad (9)$$

- **Jaccard Similarity (JC) (Liben-Nowell & Kleinberg, 2007):** The JC score is a classic measure of similarity between two neighborhood sets, which is defined as the ratio of the intersection of two neighborhood sets to the union of these two sets:

$$\text{JC}(i, j) = \frac{|\mathcal{N}_i^1 \cap \mathcal{N}_j^1|}{|\mathcal{N}_i^1 \cup \mathcal{N}_j^1|} \quad (10)$$

Let $L = 1$ and set $f(\{\mathcal{N}_k^1 | k \in P_{ji}^{2l}\}) = |\mathcal{N}_i^1 \cup \mathcal{N}_j^1|$, then we have:

$$\phi_u^L(j) = \frac{1}{|\mathcal{N}_u^1|} \sum_{i \in \mathcal{N}_u^1} \beta^1 \sum_{P_{ji}^{2l} \in \mathcal{P}_{ji}^{2l}} \frac{1}{|\mathcal{N}_i^1 \cup \mathcal{N}_j^1|} = \frac{\beta^1}{|\mathcal{N}_u^1|} \sum_{i \in \mathcal{N}_u^1} \frac{|\mathcal{N}_i^1 \cap \mathcal{N}_j^1|}{|\mathcal{N}_i^1 \cup \mathcal{N}_j^1|} = \frac{\beta^1}{|\mathcal{N}_u^1|} \sum_{i \in \mathcal{N}_u^1} \text{JC}(i, j) \quad (11)$$

- **Salton Cosine Similarity (SC) (Salton, 1989):** The SC score measures the cosine similarity between the neighborhood sets of two nodes:

$$\text{SC}(i, j) = \frac{|\mathcal{N}_i^1 \cap \mathcal{N}_j^1|}{\sqrt{|\mathcal{N}_i^1 \cup \mathcal{N}_j^1|}} \quad (12)$$

let $L = 1$ and set $f(\{\mathcal{N}_k^1 | k \in P_{ji}^{2l}\}) = \sqrt{|\mathcal{N}_i^1 \cup \mathcal{N}_j^1|}$, then we have:

$$\phi_u^L(j) = \frac{1}{|\mathcal{N}_u^1|} \sum_{i \in \mathcal{N}_u^1} \beta^1 \sum_{P_{ji}^{2l} \in \mathcal{P}_{ji}^{2l}} \frac{1}{\sqrt{|\mathcal{N}_i^1 \cup \mathcal{N}_j^1|}} = \frac{\beta^1}{|\mathcal{N}_u^1|} \sum_{i \in \mathcal{N}_u^1} \frac{|\mathcal{N}_i^1 \cap \mathcal{N}_j^1|}{\sqrt{|\mathcal{N}_i^1 \cup \mathcal{N}_j^1|}} = \frac{\beta^1}{|\mathcal{N}_u^1|} \sum_{i \in \mathcal{N}_u^1} \text{SC}(i, j) \quad (13)$$

- **Common Neighbors (CN) (Newman, 2001):** The CN score measures the number of common neighbors of two nodes and is frequently used for measuring the proximity between two nodes:

$$\text{CN}(i, j) = |\mathcal{N}_i^1 \cap \mathcal{N}_j^1| \quad (14)$$

Let $L = 1$ and set $f(\{\mathcal{N}_k^1 | k \in P_{ji}^{2l}\}) = 1$, then we have:

$$\phi_u^L(j) = \frac{1}{|\mathcal{N}_u^1|} \sum_{i \in \mathcal{N}_u^1} \beta^1 \sum_{P_{ji}^{2l} \in \mathcal{P}_{ji}^{2l}} 1 = \frac{\beta^1}{|\mathcal{N}_u^1|} \sum_{i \in \mathcal{N}_u^1} |\mathcal{N}_i^1 \cap \mathcal{N}_j^1| = \frac{\beta^1}{|\mathcal{N}_u^1|} \sum_{i \in \mathcal{N}_u^1} \text{CN}(i, j) \quad (15)$$

Since CN does not contain any normalization to remove the bias of degree in quantifying proximity and hence performs worse than other metrics as demonstrated by our recommendation experiments in Table 1.

- **Leicht-Holme-Nerman (LHN) (Leicht et al., 2006):** LHN is very similar to SC. However, it removes the square root in the denominator and is more sensitive to the degree of node:

$$\text{LHN}(i, j) = \frac{|\mathcal{N}_i^1 \cap \mathcal{N}_j^1|}{|\mathcal{N}_i^1| \cdot |\mathcal{N}_j^1|} \quad (16)$$

Let $L = 1$ and set $f(\{\mathcal{N}_k^1 | k \in P_{ji}^{2l}\}) = |\mathcal{N}_i^1| \cdot |\mathcal{N}_j^1|$, then we have:

$$\phi_u^L(j) = \frac{1}{|\mathcal{N}_u^1|} \sum_{i \in \mathcal{N}_u^1} \beta^1 \sum_{P_{ji}^{2l} \in \mathcal{P}_{ji}^{2l}} \frac{1}{|\mathcal{N}_i^1| \cdot |\mathcal{N}_j^1|} = \frac{\beta^1}{|\mathcal{N}_u^1|} \sum_{i \in \mathcal{N}_u^1} \frac{|\mathcal{N}_i^1 \cap \mathcal{N}_j^1|}{|\mathcal{N}_i^1| \cdot |\mathcal{N}_j^1|} = \frac{\beta^1}{|\mathcal{N}_u^1|} \sum_{i \in \mathcal{N}_u^1} \text{LHN}(i, j) \quad (17)$$

We further emphasize that our proposed CIR is a generalized version of these four existing metrics and can be delicately designed toward satisfying downstream tasks and datasets. We leave such exploration on the choice of f as one potential future work.

A.3 THEORETICAL PROOF

This section will thoroughly prove all derivations and theorems in this work. More specifically, Eq. (2) and Theorem 2.

A.3.1 DERIVATION OF EQUATION 2

The matrix form of computing the ranking of user u over item i after L -layer LightGCN-based message-passing:

$$y_{ui}^L = \left(\sum_{l_1=0}^L \beta_{l_1} \mathbf{E}_u^{l_1} \right)^\top \left(\sum_{l_1=0}^L \beta_{l_1} \mathbf{E}_i^{l_1} \right) = \left(\sum_{l_1=0}^L \beta_{l_1} \tilde{\mathbf{A}}^{l_1} \mathbf{E}^0 \right)_u^\top \left(\sum_{l_1=0}^L \beta_{l_1} \tilde{\mathbf{A}}^{l_1} \mathbf{E}^0 \right)_i. \quad (18)$$

where β_{l_1} is the layer contribution and LightGCN uses mean-pooling, i.e., $\frac{1}{L}$ in Eq. (7). For the propagated embedding at a specific layer l_1 , we have:

$$\mathbf{E}_u^{l_1} = (\tilde{\mathbf{A}}^{l_1} \mathbf{E}^0)_u = \sum_{j \in \mathcal{V}_u^{l_1}} \alpha_{ju}^{l_1} \mathbf{e}_j^0, \quad (19)$$

where $\alpha_{ju}^{l_1} = \sum_{P_{ju}^{l_1} \in \mathcal{P}_{ju}^{l_1}} \prod_{e_{pq} \in P_{ju}^{l_1}} d_p^{-0.5} d_q^{-0.5}$ ($\alpha_{ju}^{l_1} = 0$ if $\mathcal{P}_{ju}^{l_1} = \emptyset$). $\mathcal{V}_u^{l_1}$ is the set of all nodes having paths of length l_1 to u and can be expressed as:

$$\mathcal{V}_u^{l_1} = \bigcup_{l_2=0}^{l_1} \mathcal{N}_u^{l_2} \cdot \mathbf{1}[(l_1 - l_2) \% 2 = 0], \quad (20)$$

where

$$\mathcal{N}_u^{l_2} \cdot \mathbf{1}[(l_1 - l_2) \% 2 = 0] = \begin{cases} \mathcal{N}_u^{l_2}, & (l_1 - l_2) \% 2 = 0 \\ \emptyset, & (l_1 - l_2) \% 2 \neq 0 \end{cases}. \quad (21)$$

Substituting Eq. (20) into Eq. (19), we have:

$$\mathbf{E}_u^{l_1} = (\tilde{\mathbf{A}}^{l_1} \mathbf{E}^0)_u = \sum_{j \in \mathcal{V}_u^{l_1}} \alpha_{ju}^{l_1} \mathbf{e}_j^0 = \sum_{j \in \bigcup_{l_2=0}^{l_1} \mathcal{N}_u^{l_2} \cdot \mathbf{1}[(l_1 - l_2) \% 2 = 0]} \alpha_{ju}^{l_1} \mathbf{e}_j^0 = \sum_{l_2=0}^{l_1} \sum_{j \in \mathcal{N}_u^{l_2} \cdot \mathbf{1}[(l_1 - l_2) \% 2 = 0]} \alpha_{ju}^{l_1} \mathbf{e}_j^0. \quad (22)$$

Then the aggregation of all L layers' embeddings of user u is expressed as:

$$\sum_{l_1=0}^L \beta_{l_1} \mathbf{E}_u^{l_1} = \sum_{l_1=0}^L \beta_{l_1} \sum_{l_2=0}^{l_1} \sum_{j \in \mathcal{N}_u^{l_2} \cdot \mathbf{1}[(l_1 - l_2) \% 2 = 0]} \alpha_{ju}^{l_1} \mathbf{e}_j^0. \quad (23)$$

(23) means that for each length $l_1 \in \{0, 1, \dots, L\}$, for each node $j \in \mathcal{V}_u^{l_1}$ that has path of length l_1 to u , we propagate its embedding over each path $P_{ju}^{l_1} \in \mathcal{P}_{ju}^{l_1}$ with the corresponding weight coefficient $\prod_{e_{pq} \in P_{ju}^{l_1}} d_p^{-0.5} d_q^{-0.5}$.

Since nodes that are l_1 -hops away from u cannot have paths of length less than l_1 , we reorganize Eq. (23) by first considering the hop of each node and then considering the length of each path, which leads to:

$$\sum_{l_1=0}^L \beta_{l_1} \mathbf{E}_u^{l_1} = \sum_{l_1=0}^L \beta_{l_1} \sum_{l_2=0}^{l_1} \sum_{j \in \mathcal{N}_u^{l_2} \cdot \mathbb{1}[(l_1-l_2)\%2]} \alpha_{ju}^{l_2} \mathbf{e}_j^0 = \sum_{l_1=0}^L \sum_{j \in \mathcal{N}_u^{l_1}} \sum_{l_2=l_1}^L \beta_{l_2} \alpha_{ju}^{l_2} \mathbf{e}_j^0, \quad (24)$$

where $\alpha_{ju}^{l_2} = \sum_{P_{ju}^{l_2} \in \mathcal{P}_{ju}^{l_2}} \prod_{e_{pq} \in P_{ju}^{l_2}} d_p^{-0.5} d_q^{-0.5}$ ($\alpha_{ju}^{l_2} = 0$ if $\mathcal{P}_{ju}^{l_2} = \emptyset$). Then by substituting Eq. (24) into Eq. (18), we end up with:

$$y_{ui}^L = \left(\sum_{l_1=0}^L \sum_{j \in \mathcal{N}_u^{l_1}} \sum_{l_2=l_1}^L \beta_{l_2} \alpha_{ju}^{l_2} \mathbf{e}_j^0 \right)^\top \left(\sum_{l_1=0}^L \sum_{v \in \mathcal{N}_i^{l_1}} \sum_{l_2=l_1}^L \beta_{l_2} \alpha_{vi}^{l_2} \mathbf{e}_v^0 \right), \quad (25)$$

where $\mathcal{N}_u^0 = \{u\}$ and specifically, $\alpha_{uu}^0 = 1$. β_{l_2} is the weight measuring contributions of propagated embeddings at layer l_2 .

We further leverage an example to demonstrate the correctness of Eq. (25). We compute user u 's ranking over item i after 1-layer message-passing by setting $L = 1$:

$$\begin{aligned} y_{ui}^1 &= (\beta_0 \mathbf{e}_u^0 + \beta_1 \sum_{j \in \mathcal{N}_u^1} \alpha_{ju}^1 \mathbf{e}_j^0)^\top (\beta_0 \mathbf{e}_i^0 + \beta_1 \sum_{v \in \mathcal{N}_i^1} \alpha_{vi}^1 \mathbf{e}_v^0) = \underbrace{\beta_0^2 \mathbf{e}_u^0 \top \mathbf{e}_i^0}_{I(\mathcal{N}_u^0, \mathcal{N}_i^0)} + \\ &\underbrace{\beta_0 \beta_1 \sum_{v \in \mathcal{N}_i^1} \alpha_{vi}^1 \mathbf{e}_u^0 \top \mathbf{e}_v^0}_{I(\mathcal{N}_u^0, \mathcal{N}_i^1)} + \underbrace{\beta_0 \beta_1 \sum_{j \in \mathcal{N}_u^1} \alpha_{ju}^1 \mathbf{e}_j^0 \top \mathbf{e}_i^0}_{I(\mathcal{N}_u^1, \mathcal{N}_i^0)} + \underbrace{\beta_1^2 \sum_{j \in \mathcal{N}_u^1} \sum_{v \in \mathcal{N}_i^1} \alpha_{ju}^1 \alpha_{vi}^1 \mathbf{e}_j^0 \top \mathbf{e}_v^0}_{I(\mathcal{N}_u^1, \mathcal{N}_i^1)}, \end{aligned} \quad (26)$$

where $I(\mathcal{N}_u^{l_1}, \mathcal{N}_i^{l_2})$ represents the interactions between nodes in $\mathcal{N}_u^{l_1}$ and nodes in $\mathcal{N}_i^{l_2}$.

A.3.2 EXPRESSIVENESS OF CAGCN

Here we thoroughly prove that when g is set to be MLP, CAGCN can be more expressive than 1-WL. First, we review the concepts of subtree-isomorphism and subgraph-isomorphism.

Definition 3. Subtree-isomorphism (Wijesinghe & Wang, 2021): \mathcal{S}_u and \mathcal{S}_i are subtree-isomorphic, denoted as $\mathcal{S}_u \cong_{\text{subtree}} \mathcal{S}_i$, if there exists a bijective mapping $h : \tilde{\mathcal{N}}_u^1 \rightarrow \tilde{\mathcal{N}}_i^1$ such that $h(u) = i$ and $\forall v \in \tilde{\mathcal{N}}_u^1, h(v) = j, \mathbf{e}_v^l = \mathbf{e}_j^l$.

Definition 4. Subgraph-isomorphism (Wijesinghe & Wang, 2021): \mathcal{S}_u and \mathcal{S}_i are subgraph-isomorphic, denoted as $\mathcal{S}_u \cong_{\text{subgraph}} \mathcal{S}_i$, if there exists a bijective mapping $h : \tilde{\mathcal{N}}_u^1 \rightarrow \tilde{\mathcal{N}}_i^1$ such that $h(u) = i$ and $\forall v_1, v_2 \in \tilde{\mathcal{N}}_u^1, e_{v_1 v_2} \in \mathcal{E}_{\mathcal{S}_u}$ iff $e_{h(v_1)h(v_2)} \in \mathcal{E}_{\mathcal{S}_i}$ and $\mathbf{e}_{v_1}^l = \mathbf{e}_{h(v_1)}^l, \mathbf{e}_{v_2}^l = \mathbf{e}_{h(v_2)}^l$.

Then we theoretically demonstrate the equivalence between the subtree-isomorphism and the subgraph-isomorphism in bipartite graphs:

Theorem 1. In bipartite graphs, two subgraphs that are subtree-isomorphic if and only if they are subgraph-isomorphic.

Proof. We prove this theorem in two directions. Firstly (\implies), we prove that in a bipartite graph, two subgraphs that are subtree-isomorphic are also subgraph-isomorphic by contradiction. Assuming that there exists two subgraphs $\mathcal{S}_u, \mathcal{S}_i$ that are subtree-isomorphic yet not subgraph-isomorphic in a bipartite graph, i.e., $\mathcal{S}_u \cong_{\text{subtree}} \mathcal{S}_i, \mathcal{S}_u \not\cong_{\text{subgraph}} \mathcal{S}_i$. By definition of subtree-isomorphism, we trivially have $\mathbf{e}_v^l = \mathbf{e}_{h(v)}^l, \forall v \in \mathcal{V}_{\mathcal{S}_u}$. Then to guarantee $\mathcal{S}_u \not\cong_{\text{subgraph}} \mathcal{S}_i$ and also since edges are only allowed to connect u and its neighbors \mathcal{N}_u^1 in the bipartite graph, there must exist at least

an edge e_{uv} between u and one of its neighbors $v \in \mathcal{N}_u^1$ such that $e_{uv} \in \mathcal{E}_{S_u}, e_{h(u)h(v)} \notin \mathcal{E}_{S_i}$, which contradicts the assumption that $S_u \cong_{\text{subtree}} S_i$. Secondly (\Leftarrow), we can prove that in a bipartite graph, two subgraphs that are subgraph-isomorphic are also subtree-isomorphic, which trivially holds since in any graph, subgraph-isomorphism leads to subtree-isomorphism (Wijesinghe & Wang, 2021). \square

Since 1-WL test can distinguish subtree-isomorphic graphs (Wijesinghe & Wang, 2021), the equivalence between these two isomorphisms indicates that in bipartite graphs, both of the subtree-isomorphic graphs and subgraph-isomorphic graphs can be distinguished by 1-WL test. Therefore, to go beyond 1-WL in bipartite graphs, we propose a novel bipartite-subgraph-isomorphism in Definition 2, which is even harder to be distinguished than the subgraph-isomorphism by 1-WL test:

Definition 2. Bipartite-subgraph-isomorphism: S_u and S_i are bipartite-subgraph-isomorphic, denoted as $S_u \cong_{\text{bi-subgraph}} S_i$, if there exists a bijective mapping $h : \tilde{\mathcal{N}}_u^1 \cup \mathcal{N}_u^2 \rightarrow \tilde{\mathcal{N}}_i^1 \cup \mathcal{N}_i^2$ such that $h(u) = i$ and $\forall v, v' \in \tilde{\mathcal{N}}_u^1 \cup \mathcal{N}_u^2, e_{vv'} \in \mathcal{E} \iff e_{h(v)h(v')} \in \mathcal{E}$ and $\mathbf{e}_v^l = \mathbf{e}_{h(v)}^l, \mathbf{e}_{v'}^l = \mathbf{e}_{h(v')}^l$.

With the bipartite-subgraph-isomorphism defined, we prove the injective property in the following:

Lemma 1. *If g is MLP, then $g(\{(\gamma_i \tilde{\Phi}_{ij}, \mathbf{e}_j^l) | j \in \mathcal{N}_i^1\}, \{(d_i^{-0.5} d_j^{-0.5}, \mathbf{e}_j^l) | j \in \mathcal{N}_i^1\})$ is injective.*

Proof. If we assume that all node embeddings share the same discretization precision, then embeddings of all nodes in a graph can form a countable set \mathcal{H} . Similarly, for each edge in a graph, its CIR-based weight $\tilde{\Phi}_{ij}$ and degree-based weight $d_i^{-0.5} d_j^{-0.5}$ can also form two different countable sets $\mathcal{W}_1, \mathcal{W}_2$ with $|\mathcal{W}_1| = |\mathcal{W}_2|$. Then $\mathcal{P}_1 = \{\tilde{\Phi}_{ij} \mathbf{e}_i | \tilde{\Phi}_{ij} \in \mathcal{W}_1, \mathbf{e}_i \in \mathcal{H}\}, \mathcal{P}_2 = \{d_i^{-0.5} d_j^{-0.5} \mathbf{e}_i | d_i^{-0.5} d_j^{-0.5} \in \mathcal{W}_2, \mathbf{e}_i \in \mathcal{H}\}$ are also two countable sets. Let P_1, P_2 be two multisets containing elements from \mathcal{P}_1 and \mathcal{P}_2 , respectively, and $|P_1| = |P_2|$. Then by Lemma 1 in (Wijesinghe & Wang, 2021), there exists a function f such that $\pi(P_1, P_2) = \sum_{p_1 \in P_1, p_2 \in P_2} f(p_1, p_2)$ is unique for any distinct pair of multisets (P_1, P_2) . Since the MLP-based g is a universal approximator (Xu et al., 2018) and hence can learn the function f , we know that g is injective. \square

Theorem 2. *Let M be a GNN with sufficient number of CAGC-based convolution layers defined by Eq. (5). If g is MLP, then M is strictly more expressive than 1-WL in distinguishing subtree-isomorphic yet non-bipartite-subgraph-isomorphic graphs.*

Proof. We prove this theorem in two directions. Firstly (\implies), following (Wijesinghe & Wang, 2021), we prove that the designed CAGCN here can distinguish any two graphs that are distinguishable by 1-WL by contradiction. Assume that there exist two graphs \mathcal{G}_1 and \mathcal{G}_2 which can be distinguished by 1-WL but cannot be distinguished by CAGCN. Further, suppose that 1-WL cannot distinguish these two graphs in the iterations from 0 to $L-1$, but can distinguish them in the L^{th} iteration. Then, there must exist two neighborhood subgraphs S_u and S_i whose neighboring nodes correspond to two different sets of node labels at the L^{th} iteration, i.e., $\{\mathbf{e}_v^l | v \in \mathcal{N}_u^1\} \neq \{\mathbf{e}_j^l | j \in \mathcal{N}_i^1\}$. Since g is injective by Lemma 1, for S_u and S_i , g would yield two different feature vectors at the L^{th} iteration. This means that CAGCN can also distinguish \mathcal{G}_1 and \mathcal{G}_2 , which contradicts the assumption.

Secondly (\impliedby), we prove that there exist at least two graphs that can be distinguished by CAGCN but cannot be distinguished by 1-WL. Figure 7 presents two of such graphs S_u, S'_u , which are subgraph isomorphic but non-bipartite-subgraph-isomorphic. Assuming u and u' have exactly the same neighborhood feature vectors \mathbf{e} , then directly propagating according to 1-WL or even considering node degree as the edge weight as GCN (Kipf & Welling, 2017) can still end up with the same propagated feature for u and u' . However, if we leverage JC as calculate CIR as introduced in Appendix A.2, then we would end up with $\{(d_u d_{j_1})^{-0.5} \mathbf{e}, (d_u d_{j_2})^{-0.5} \mathbf{e}, (d_u d_{j_3})^{-0.5} \mathbf{e}\} \neq \{(d_{u'}^{-0.5} d_{j'_1}^{-0.5} + \tilde{\Phi}_{u'j'_1}) \mathbf{e}, (d_{u'}^{-0.5} d_{j'_2}^{-0.5} + \tilde{\Phi}_{u'j'_2}) \mathbf{e}, (d_{u'}^{-0.5} d_{j'_3}^{-0.5} + \tilde{\Phi}_{u'j'_3}) \mathbf{e}\}$. Since g is injective by Lemma 1, CAGCN would yield two different embeddings for u and u' . \square

Theorem 2 indicates that GNNs whose aggregation scheme is CAGC can distinguish non-bipartite-subgraph-isomorphic graphs that are indistinguishable by 1-WL.

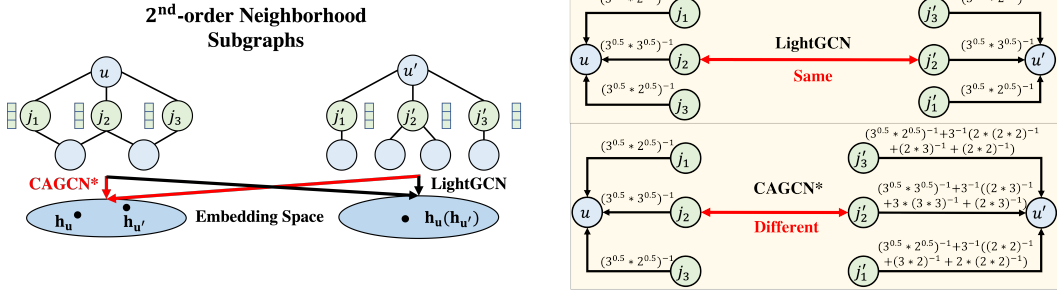


Figure 7: An example showing two neighborhood subgraphs $\mathcal{S}_u, \mathcal{S}_{u'}$ that are subgraph-isomorphic but not bipartite-subgraph-isomorphic.

A.4 APPROXIMATION OF CIR

Here we expect to demonstrate that for each center node, its neighbors with higher interactions with its whole neighborhood would also have higher interactions with its to-be-predicted neighbors in the testing set. To verify it, we define the to-be-predicted neighborhood set of user u in the testing set as $\hat{\mathcal{N}}_u^1$ and for each neighbor $j \in \mathcal{N}_u^1$, calculate its CIR with nodes in $\hat{\mathcal{N}}_u^1$ as follows:

$$\hat{\phi}_u^L(j) = \frac{1}{|\hat{\mathcal{N}}_u^1|} \sum_{i \in \hat{\mathcal{N}}_u^1} \sum_{l=1}^L \beta^{2l} \sum_{P_{ji}^{2l} \in \mathcal{P}_{ji}^{2l}} \frac{1}{f(\{\mathcal{N}_k^1 | k \in P_{ji}^{2l}\})}, \forall j \in \mathcal{N}_u^1, \forall u \in \mathcal{U}, \quad (27)$$

Then we compare the ranking consistency among CIRs calculated from training neighborhoods (i.e., $\phi_u(j)$), from testing neighborhoods (i.e., $\hat{\phi}_u(j)$) and from full neighborhoods (we replace $\hat{\mathcal{N}}_u^1$ with $\mathcal{N}_u^1 \cup \hat{\mathcal{N}}_u^1$ in Eq. (27)). Here we respectively use four topological metrics (JC, SC, LHN, and CN) to define f and rank the obtained three lists. Then, we measure the similarity of the ranked lists between Train-Test and between Train-Full by Rank-Biased Overlap (RBO) (Webber et al., 2010). The averaged RBO values over all nodes $v \in \mathcal{V}$ on three datasets are shown in Table 4. We can clearly see that the RBO values on all these datasets using all topological metrics are beyond 0.5, which verifies our approximation. The RBO value between Train-Full is always higher than the one between Train-Test because most interactions are in the training set.

Table 4: Average Rank-Biased Overlap (RBO) of the ranked neighbor lists between training (i.e., \mathcal{N}_u^1) and testing/full (i.e., $\hat{\mathcal{N}}_u^1$ and $\mathcal{N}_u^1 \cup \hat{\mathcal{N}}_u^1$, respectively) dataset over all nodes $u \in \mathcal{U}$

Metric	Gowalla		Yelp		MI-1M	
	Train-Test	Train-Full	Train-Test	Train-Full	Train-Test	Train-Full
JC	0.604±0.129	0.902±0.084	0.636±0.124	0.897±0.081	0.848±0.092	0.978±0.019
SC	0.611±0.127	0.896±0.084	0.657±0.124	0.900±0.077	0.876±0.077	0.983±0.015
LHN	0.598±0.121	0.974±0.036	0.578±0.100	0.976±0.029	0.845±0.082	0.987±0.009
CN	0.784±0.120	0.979±0.029	0.836±0.100	0.983±0.023	0.957±0.039	0.995±0.006

A.5 MODEL ARCHITECTURE AND COMPLEXITY OF CAGCN

A.5.1 ARCHITECTURE

The model architecture of our CAGCN is shown in Figure 8. We take a specific example of computing the ranking of user u over item i . We first calculate the estimated CIR of each neighbor with respect to the rest of the corresponding neighborhoods as Eq. (5) and then we iteratively propagate neighbors' embeddings with the awareness of the collaboration benefits by following the calculated CIR. Then we weighted combine the propagated embeddings at each layer to obtain the aggregated embedding for u and i as Eq. (6). After that, we calculate their ranking based on the dot-product similarity. The optimization of CAGCN is the same as LightGCN in Eq. (8).

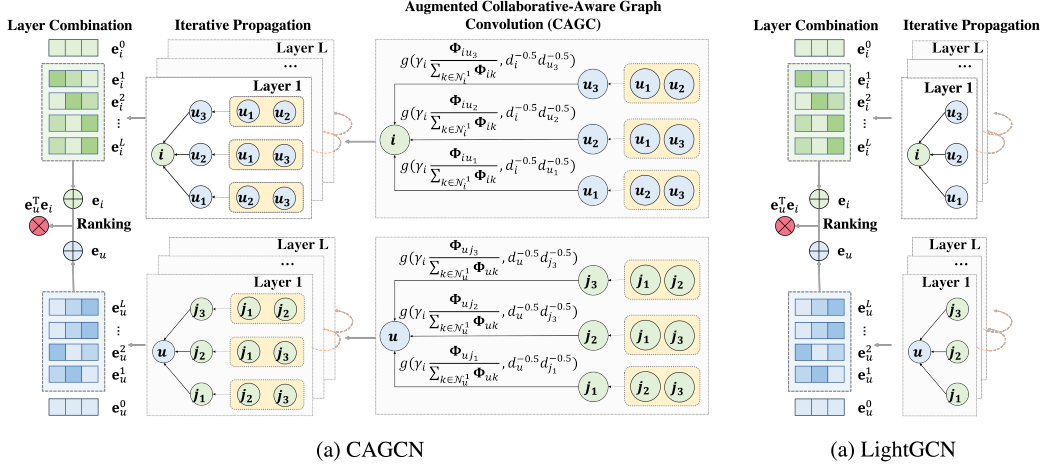


Figure 8: Comparing the model architecture of CAGCN and LightGCN.

A.5.2 COMPLEXITY COMPARISON

Here we thoroughly compare the time/space complexity of our model and existing baselines. Let $|\mathcal{V}|$, $|\mathcal{E}|$, $|\mathcal{F}|$ be the total number of nodes, edges, and feature dimensions (assuming feature dimensions stay the same after feature transformation of any neural layer). Let L be the propagation layer for all graph-based models involving message-passing. Specifically for UltraGCN, since it samples a large number of pairs per epoch per positive pair, we cannot ignore such complexity as compared to other baselines. Let r be the total number of negative samples per epoch per positive pair and K be the number of 2^{nd} -order neighbors. We exclude the basic hyperparameters used for all models, which include l_2 regularization coefficient, learning rate, batch size, and training epochs. For the number of negative samples, aside from UltraGCN, all other baselines use 1 per epoch per positive pair. Then the complexity of each model is summarized as follows:

Table 5: Complexity of the pre-processing and the forward pass of CAGCN and different baselines.

Model	MF	NGCF	LightGCN	UltraGCN	CAGCN
# Extra Hyper-parameters	/	/	1	7	2
Preprocess	Space	$\mathcal{O}(\mathcal{E} + \mathcal{V})$	$\mathcal{O}(\mathcal{E} + \mathcal{V})$	$\mathcal{O}(\mathcal{E} + \mathcal{V})$	$\mathcal{O}(\mathcal{E} + \mathcal{V})$
	Time	$\mathcal{O}(\mathcal{E} + \mathcal{V})$	$\mathcal{O}(\mathcal{E} + \mathcal{V})$	$\mathcal{O}(\mathcal{V} ^3)$	$\mathcal{O}(\mathcal{V} ^3)$
Training	Space	$\mathcal{O}(L \mathcal{V} F + \mathcal{E} + LF^2)$	$\mathcal{O}(L \mathcal{V} F + \mathcal{E})$	$\mathcal{O}(\mathcal{V} F + \mathcal{V} K)$	$\mathcal{O}(L \mathcal{V} F + \mathcal{E})$
	Time	$\mathcal{O}(L \mathcal{E} F + \mathcal{V} F^2)$	$\mathcal{O}(L \mathcal{E} F + L \mathcal{V} F)$	$\mathcal{O}(r(\mathcal{E} + \mathcal{V} K)F)$	$\mathcal{O}(L \mathcal{E} F + L \mathcal{V} F)$

Generally compared with the very basic MF, the main computational issue of LightGCN comes from the message-passing which takes $\mathcal{O}(L|\mathcal{E}|F)$ time and $\mathcal{O}(L|\mathcal{V}|F)$ space to save the intermediate node representations. For NGCF, the extra complexity comes from the nonlinear transformation, which takes $\mathcal{O}(L|\mathcal{V}|F^2)$ time and $\mathcal{O}(LF^2)$ space to save the transformation weights. For UltraGCN, the main bottleneck comes from computing the user-user connections, which involves the power of adjacency matrix and hence $\mathcal{O}(|\mathcal{V}|^3)$. Furthermore, as it samples hundreds of negative samples and the optimization is also performed on the user-user connections, then its time complexity would be $\mathcal{O}(r(|\mathcal{E}| + |\mathcal{V}|K)F)$.

A.6 EXPERIMENTAL SETTING

A.6.1 DATASETS

Following (He et al., 2020; Wang et al., 2019), we validate the proposed approach on four widely used benchmark datasets in recommender systems, including **Gowalla**, **Yelp**, **Amazon**, and **MI-1M**, the details of which are provided in (He et al., 2020; Wang et al., 2019). Moreover, we collect two extra datasets to further demonstrate the superiority of our proposed model in even broader user-item

interaction domains: **(1) Loseit**: This dataset is collected from subreddit *loseit - Lose the Fat*⁴ from March 2020 to March 2022 where users discuss healthy and sustainable methods of losing weight via posts. To ensure the quality of this dataset, we use the 10-core setting to filter out cold-start users (He & McAuley, 2016), i.e., retaining users and posts with at least ten interactions. **(2) News**: This dataset includes the interactions from subreddit *World News*⁵ where users share major news around the world via posts. Similarly, we use the 10-core setting to ensure the quality of this dataset. We summarize the statistics of all six datasets in Table 6.

Table 6: Basic dataset statistics.

Dataset	# Users	# Items	# Interactions	Density
Gowalla	29, 858	40, 981	1, 027, 370	0.084%
Yelp	31, 668	38, 048	1, 561, 406	0.130%
Amazon	52, 643	91, 599	2, 984, 108	0.062%
MI-1M	6, 022	3, 043	895, 699	4.888%
Loseit	5, 334	54, 595	230, 866	0.08%
News	29, 785	21, 549	766, 874	0.119%

A.6.2 BASELINES

We compare our proposed CAGCN(*) with the following baselines:

- **MF (Rendle et al., 2012)**: This is the most classic collaborative filtering method equipped with the BPR loss, which preserves users’ ranking over interacted items.
- **NGCF (Wang et al., 2019)**: This was the very first GNN-based collaborative filtering model to incorporate high-order connectivity of user-item interactions for the recommendation.
- **LightGCN (He et al., 2020)**: This is the most popular collaborative filtering model based on GNNs, which extends NGCF by removing feature transformation and nonlinear activation, and achieves a better trade-off between performance and efficiency.
- **UltraGCN (Mao et al., 2021)**: This model simplifies GCNs for collaborative filtering by omitting infinite layers of message passing for the efficient recommendation, and it constructs the user-user graphs to leverage higher-order relationships. Thus, it achieves both better performance and shorter running time than LightGCN.
- **GTN (Fan et al., 2021)**: This model leverages a robust and adaptive propagation based on the trend of the aggregated messages to avoid unreliable user-item interactions.

Note that here we only compare the proposed CAGCN(*) with the baselines that focus on the operation of graph convolution (besides the classic MF) including the state-of-the-art GNN-based recommendation models (i.e., UltraGCN and GTN). There are some other developing methodology directions (e.g., Fu et al. (2022); Chen et al. (2022b;a; 2021)) that can obtain comparable results to the aforementioned baselines on some of the benchmark datasets. However, these methods are either not GNN-based Fu et al. (2022) or incorporate some other general machine learning techniques rather than focus on graph convolution, e.g., SGCN Chen et al. (2021) leverages the stochastic binary masks to remove noisy edges, and GOTNet Chen et al. (2022a) performs k-Means clustering on nodes’ embeddings to capture long-range dependencies. Given our main focus is on advancing the frontier of graph-convolution in recommendation systems, we omit these other comparable baselines. Note that our work could be further enhanced if we incorporate these general machine learning techniques but we leave this as one future direction.

A.6.3 CAGCN-VARIANTS

For CAGCN, we set $\gamma_i = \sum_{r \in \mathcal{N}_i^1} d_i^{-0.5} d_r^{-0.5}$ to ensure that the total edge weights for messages received by each node are the same as LightGCN. Therefore, Eq. 5 for CAGCN becomes:

$$\mathbf{e}_i^{l+1} = \sum_{j \in \mathcal{N}_i^1} \left(\left(\sum_{r \in \mathcal{N}_i^1} d_i^{-0.5} d_r^{-0.5} \right) \frac{\Phi_{ij}}{\sum_{k \in \mathcal{N}_i^1} \Phi_{ik}} \right) \mathbf{e}_j^l, \forall i \in \mathcal{V}. \quad (28)$$

⁴<https://www.reddit.com/r/loseit/>

⁵<https://www.reddit.com/r/worldnews/>

For CAGCN*, we set $\gamma_i = \gamma$ as a constant controlling the trade-off between contributions from message-passing according to LightGCN and according to CAGC. Eq. 5 for CAGCN* becomes:

$$\mathbf{e}_i^{l+1} = \sum_{j \in \mathcal{N}_i^1} (\gamma \frac{\Phi_{ij}}{\sum_{k \in \mathcal{N}_i^1} \Phi_{ik}} + d_i^{-0.5} d_j^{-0.5}) \mathbf{e}_j^l, \forall i \in \mathcal{V}, \quad (29)$$

where we search γ in $\{1, 1.2, 1.5, 1.7, 2.0\}$.

A.6.4 EXPERIMENTAL SETUP AND HYPERPARAMETERS.

Following LightGCN (He et al., 2020) and NGCF (Wang et al., 2019), we select 80% historical interactions as the training set and 20% as the testing set. The best performance is achieved when the training loss does not decrease for 100 epochs any more. Two popular metrics: Recall@K and Normalized Discounted Cumulative Gain (NDCG@K) Wang et al. (2019) are adopted to evaluate all models. We set the default value of K as 20 and report the average of Recall@20 and NDCG@20 over all users in the test set. In the inference phase, we treat items that the user has never interacted with in the training set as candidate items. All recommendation models predict the user’s preference scores over these candidate items and rank them based on the computed scores to further calculate Recall@20 and NDCG@20.

We list the hyperparameters used for each baseline and our model as follows:

- **LightGCN.** Propagation layers: $L = 3$; Pooling layer: Meaning pooling;
- **NGCF.** Propagation layers: $L = 3$; Slope of LeakyRelu: 0.2; Pooling layer: Concatenation
- **UltraGCN.** For Gowalla, Yelp, Amazon and MI-1M, we use exactly the same hyperparameter configurations provided here. For Loseit and News, the hyperparameters are as follows:
 - (1) Loseit: Training epochs 2000; Learning rate $1e^{-3}$; batch size 512; Loss weights $w_1 = 1e^{-6}, w_2 = 1, w_3 = 1e^{-6}, w_4 = 1$; the number of negative samples per epoch per positive pair 20; negative weight 20; weight of l_2 regularization $\gamma = 1e^{-4}$, 2^{nd} -constraining loss coefficient $\lambda = 5e^{-4}$.
 - (2) News: Training epochs 2000; Learning rate $1e^{-3}$; batch size 1024; Loss weights $w_1 = 1e^{-8}, w_2 = 1, w_3 = 1, w_4 = 1e^{-8}$; the number of negative samples per epoch per positive pair 1000; negative weight 200; weight of l_2 regularization $\gamma = 1e^{-4}$, 2^{nd} -constraining loss coefficient $\lambda = 5e^{-4}$.
- **GTN.** For Gowalla, Yelp, Amazon, we directly report the result provided here.

In the following, we introduce the hyperparameters we used for our CAGCN(*)-variants. With specification, the number of training epochs is set to be 1000; the learning rate 0.001; l_2 regularization $1e^{-4}$; number of negative samples 1; embedding dimension 64; batch size 256.
- **CAGCN-jc.** (1) Gowalla: $\gamma = 1$; (2) Yelp: $\gamma = 1.2$; (3) Amazon: $\gamma = 1$; (4) MI-1M: $\gamma = 2$; (5) Loseit: $\gamma = 1$; (6) News: $\gamma = 1$.
- **CAGCN-cn.** (1) Gowalla: $\gamma = 1$; (2) Yelp: $\gamma = 1.2$; (3) Amazon: $\gamma = 1$; (4) MI-1M: $\gamma = 1$; (5) Loseit: $\gamma = 1$; (6) News: $\gamma = 1$.
- **CAGCN-sc.** (1) Gowalla: $\gamma = 1$; (2) Yelp: $\gamma = 1$; (3) Amazon: $\gamma = 1$; (4) MI-1M: $\gamma = 2$; (5) Loseit: $\gamma = 1$; (6) News: $\gamma = 1$.
- **CAGCN-lhn.** (1) Gowalla: $\gamma = 1.2$; (2) Yelp: $\gamma = 1$; (3) Amazon: $\gamma = 1$; (4) MI-1M: $\gamma = 2$; (5) Loseit: $\gamma = 1, L = 1$; (6) News: $\gamma = 1.5$.
- **CAGCN*-jc.** (1) Gowalla: $\gamma = 1.2, l_2$ -regularization $1e^{-3}$; (2) Yelp: $\gamma = 1.7, l_2$ -regularization $1e^{-3}$; (3) Amazon: $\gamma = 1.7, l_2$ -regularization $1e^{-3}$; (4) MI-1M: $\gamma = 1, l_2$ -regularization $1e^{-3}$; (5) Loseit: $\gamma = 1, L = 2$; (6) News: $\gamma = 1, L = 2$.
- **CAGCN*-sc.** (1) Gowalla: $\gamma = 1.2, l_2$ -regularization $1e^{-3}$; (2) Yelp: $\gamma = 1.7, l_2$ -regularization $1e^{-3}$; (3) Amazon: $\gamma = 1.7, l_2$ -regularization $1e^{-3}$; (4) MI-1M: $\gamma = 1, l_2$ -regularization $1e^{-3}$; (5) Loseit: $\gamma = 1, L = 2$; (6) News: $\gamma = 1, L = 2$.
- **CAGCN*-lhn.** (1) Gowalla: $\gamma = 1, l_2$ -regularization $1e^{-3}$; (2) Yelp: $\gamma = 1, l_2$ -regularization $1e^{-3}$; (3) Amazon: $\gamma = 1.5, l_2$ -regularization $1e^{-3}$; (4) MI-1M: $\gamma = 1, l_2$ -regularization $1e^{-3}$; (5) Loseit: $\gamma = 0.5, L = 2$; (6) News: $\gamma = 1, L = 2$.

A.7 ADDITIONAL EXPERIMENTS

A.7.1 THE PERFORMANCE OF ADDING EDGES ACCORDING TO LOCAL CIRs

Here we introduce how we add edges according to CIRs. Given the user-item interactions for training, we first construct the user-item bipartite graph and calculate the different variants of CIR including jc, sc, cn, lhn as stated in Appendix A.2. Then for each node, we rank its neighbors according to the computed CIR. In the construction stage, we first remove all edges in this bipartite graph. Then we iteratively cycle over each node and add its corresponding neighbor according to the ranking until hitting the budget. The whole flow chart is shown in Figure 9 where we have totally two users u_1, u_2 , each of which has 5 neighbors. Assuming the budget we have for adding edges is 3, then during the 1st-round, we select the top-1 neighbor for each user u_1 and u_2 and add the corresponding edge. Since we have not reached the budget, we enter into the 2nd-round and select the top-2 neighbor for each user u_1 and u_2 . Since after adding the top-2 neighbor of u_1 we have reached the budget, we stop the whole process and will not add the top-2 neighbor of u_2 .

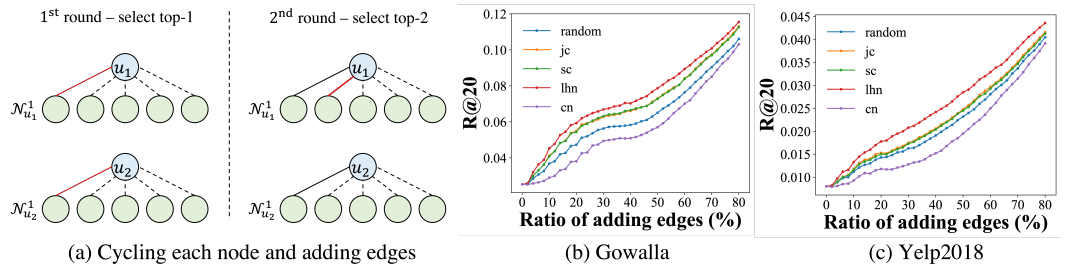


Figure 9: (a) The procedure of adding edges according to CIR of neighbors around each node. (b)-(c) The performance change of adding edges on Gowalla and Yelp2018.

Similar as what we observed in Figure 3(c)-(d), the performance increases as we add more edges on Gowalla and Yelp2018 (Figure 9(b) and (c), respectively). Furthermore, except for cn, adding edges according to CIR-variants is more effective in increasing the performance, which demonstrates the effectiveness of CIR in measuring the edge importance.

A.7.2 THE PERFORMANCE OF ADDING EDGES ACCORDING TO GLOBAL CIRs

Here we introduce how we add edges globally according to CIRs. Given the user-item interactions for training, we first construct the user-item bipartite graph and calculate the different variants of CIR including jc, sc, cn, lhn as stated in Appendix A.2. Then, we directly rank all edges according to the computed CIR. In the construction stage, we first remove all edges in this bipartite graph. Then we select top edges according to the ranking based on our budgets. The whole flow chart is shown in Figure 10(a) where we have totally two users u_1, u_2 , each of which has 5 neighbors. Assuming the budget we have for adding edges is 3, then we directly select the top-3 edges from all users' neighbors and add them to our bipartite graph.

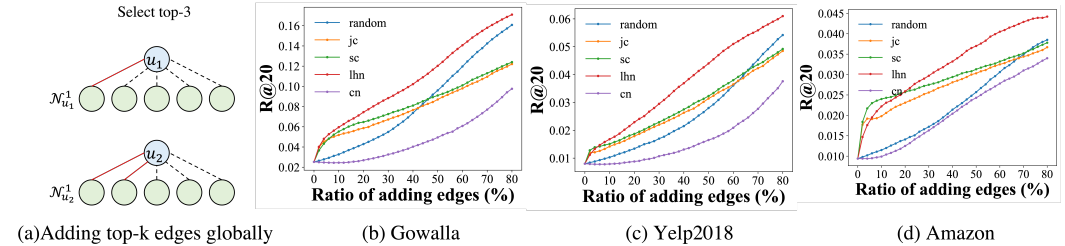


Figure 10: (a) The procedure of adding edges according to CIR of neighbors around each node. (b)-(c) The performance change of adding edges on Gowalla and Yelp2018.

In the first stage, we observe a similar trend that adding edges according to CIRs lead to faster performance gain, which demonstrate the effectiveness of CIR in measuring the edge importance

globally. However, since we don't cycle over each node and add its corresponding edge as we do in Appendix A.7.1, we would keep adding so many edges with larger CIR for the same node, which may not maximize our performance benefit when the metric is calculated by averaging over all nodes.

A.7.3 EFFICIENCY COMPARISON

Here we use exactly the same setting introduced in Appendix A.6.4 and keep track the performance/training time per 5 epochs for Gowalla, Yelp2018, MI-1M, and Loseit in Figure 11. Clearly, CAGCN* achieves extremely higher performance in significantly less time because the collaboration-aware graph convolution leverages more beneficial collaborations from neighborhoods. Specifically, in Figure 11(c), we observe the slower performance increase of CAGCN* and LightGCN on MI-1M. We ascribe this to the higher density of MI-1M as in Table 6 that leads to so much noisy neighboring information. One future direction could be to leverage the CIR to prune the graph of these noisy connections in an iterative fashion as either a preprocessing step or even used throughout training when paired with an attention mechanism (although the latter would come at a significantly longer training time).

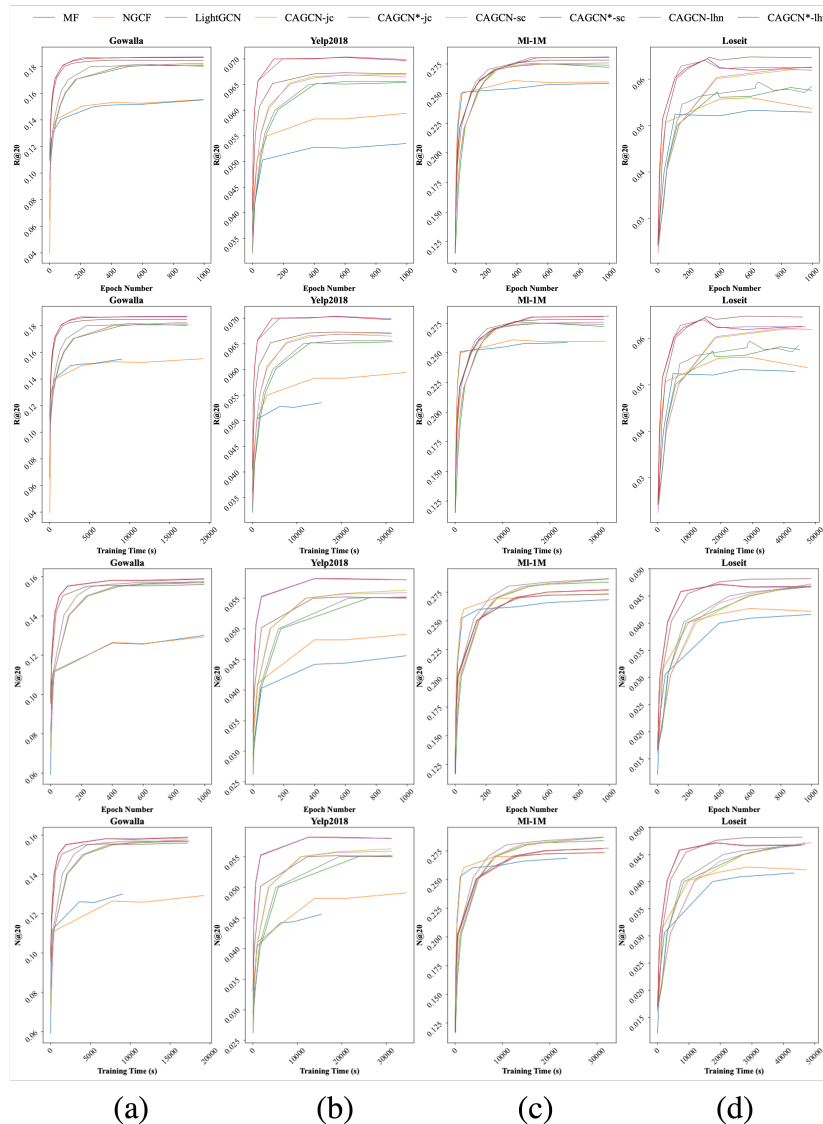


Figure 11: Comparing the training efficiency of each model under R@20 and N@20.

A.7.4 PERFORMANCE INTERPRETATION

To demonstrate the generality of our observation in Figure 5, we further perform exactly the same analysis on Yelp (shown in Figure 12) and derive almost the same insights: 1) Graph-based recommendation models achieve higher performance than non-graph-based ones for lower degree nodes; 2) the opposite performance trends between NDCG and Recall indicates that different evaluation metrics have different levels of sensitivity to node degrees.

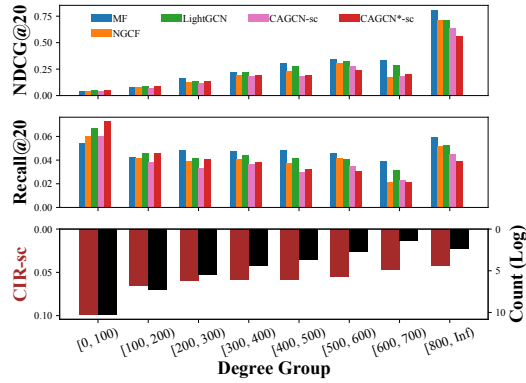


Figure 12: The performance of each model w.r.t. node degree on Yelp.